

A complex logistic equation for universal energy evolution in hadronic elastic scattering

Anderson Kendi Kohara

¹CPHT, CNRS, École Polytechnique, Institut Polytechnique de Paris, 91120 Palaiseau, France ^{*}
May 30, 2025

Abstract

We introduce a universal evolution equation for elastic scattering of hadrons, derived from Regge field theory (RFT) and solved in closed analytical form. The equation emerges from a complex logistic structure and evolves initial amplitude profiles taken from existing models at fixed energy, reproducing both the differential cross sections and the integrated quantities in a broad energy range. We prove that it admits a unique solution for each initial condition and rigorously satisfies unitarity, the Froissart-Martin bound, and dispersion relations. The dynamics are governed by two physically meaningful parameters: the effective Pomeron mass ϵ_P and the nonlinear coupling λ , both fitted at a single energy. Our approach offers a minimal, yet predictive framework for saturation and unitarization in elastic scattering and may provide a useful bridge toward small- x QCD evolution.

1 Introduction

The fundamental ingredients of matter play a crucial role in the dynamics of the interactions at high energies hadronic collisions. When hard scales are involved, perturbative techniques such as Feynman diagrams become applicable, allowing scattering amplitudes to be computed systematically. However, elastic scattering resides in the non-perturbative domain and effective descriptions must be used instead. The particles involved in the collisions pass by each other with large impact parameter and, since this is a quantum-mechanical effect, there is non zero probability that the particles will overlap their radius without fragmenting.

In problems with spherical symmetry, such as scattering, it is well known that the amplitude can be expressed through a partial wave expansion. For

^{*}email:anderson.kendi@gmail.com

axially symmetric cases, the scattering amplitude takes the form

$$A(\theta) = 16\pi \sum_{l=0}^{\infty} (2l+1) \frac{e^{i\delta_l}}{k} \sin \delta_l P_l(\cos \theta) . \quad (1)$$

Here, θ denotes the scattering angle and δ_l represents the phase shift. Geometrically, the angle of θ is related to the impact parameter between the two colliding objects, while the phase shift δ_l encodes the effect of the interaction potential between the colliding particles. Although commonly used in quantum mechanics, this decomposition is a general result that applies to wave phenomena governed by spherical symmetry, including classical wave scattering.

In relativistic scattering, the Mandelstam variables s , t , and u are used to describe the kinematics. Moreover, the scattering amplitudes must be symmetrized to account for the exchange symmetries of the system. The partial wave expansion can be analytically continued into the t -channel and reformulated as [1]

$$A^{\pm}(s, t) = 16\pi \sum_{l=0}^{\infty} (2l+1) A_l(t) \left(1 \pm e^{-i\pi l} \right) P_l(\cos \theta_t) , \quad (2)$$

with $\cos(\theta_t) = 1 + \frac{2s}{t-4m^2}$ and $A_l(t)$ carrying the phase shift information. The sign \pm refers to even and odd angular momentum in the sum. In high-energy limit the Legendre polynomial approximates to $P_l(\cos(\theta_t)) \sim s^l$. The analytic continuation of l is necessary in order to have a convergent series. This is the well-known Regge formalism and the angular momentum is replaced by the Regge trajectory [2]

$$l = \alpha(t) = \alpha_0 + \alpha' t , \quad (3)$$

describing the position of the poles in complex l -plane. For center-of-mass energies from 1 to 20 GeV, the collision energy is considered high enough to apply Regge phenomenology but not sufficiently high to be classified as a hadronic high-energy process, since resonances and bound states could still contribute to the total cross section. For the elastic scattering experiments performed within this range, the Regge phenomenology describes relatively well the behavior of total cross sections and the differential cross section near the origin, where the scattering angle is close to zero. The coefficients of the Regge trajectories found by the phenomenology give negative intercepts, leading to a decreasing total cross section with increasing energy, since in this framework the total cross section scales as $\sigma_t \sim s^{\alpha_0-1}$. Typically the Regge amplitude is written as

$$A^{\pm}(s, t) \sim 16\pi \sum_i \beta_i^{\pm}(t) \left(1 \pm e^{-i\pi\alpha_i^{\pm}(t)} \right) \left(\frac{s}{s_0} \right)^{\alpha_i^{\pm}(t)} , \quad (4)$$

where the sum runs over the specific family of Reggeons, $\beta_i^{\pm}(t)$ is the residue function describing how strongly the Regge pole contributes to the scattering amplitude and $\eta_i^{\pm} = (1 \pm e^{-i\pi\alpha_i^{\pm}(t)})$ is the signature factor.

By the end of the 1960s, the prevailing view was that the total cross section should either saturate to a constant or vanish asymptotically [3]. This view was supported by both experimental trends and the Pomeronchuk theorems. However, the Froissart-Martin bound [4,5], establishing an upper bound for the total cross section at asymptotic energies, gave an indication that an increasing cross section with increasing energy would be acceptable, at least if the strong interactions were considered a short-range interaction and the quantum probability of all possible scattering channels was conserved. Some experts, like Cheng and Wu, based on field theory of high-energy quantum electrodynamics, summing ladder diagrams predicted that the total cross section should increase with increasing energy [6], paving the way to the Pomeron interpretation. Three years later, the experiments conducted by Tevatron at FERMILAB and ISR at CERN [7,8] were able to access energies above 20 GeV and showed that the total cross section $\sigma_{\text{tot.}}$ was indeed increasing. To explain the experimental data, the phenomenology required a different kind of Regge trajectory, the Pomeron. This object has even parity across the channels pp and $p\bar{p}$, its Regge trajectory contains a positive intercept and a smaller slope compared to the standard Regge trajectories. The simple-pole Pomeron amplitude is a complex function

$$\mathcal{T}_{\mathcal{P}}(s, t) = g_a(t) g_b(t) \beta_{\mathcal{P}}(t) \left(i - \cot \frac{\pi \alpha_{\mathcal{P}}(t)}{2} \right) \left(\frac{s}{s_0} \right)^{\alpha_{\mathcal{P}}(t)}, \quad (5)$$

where $\alpha_{\mathcal{P}}(t) = 1 + \epsilon_{\mathcal{P}} + \alpha' t$ is the standard linear Pomeron trajectory with the intercept $\epsilon_{\mathcal{P}}$ and the slope α' and positive parity $\eta_{\mathcal{P}}^+ = -\sin(\pi \alpha_{\mathcal{P}}) [i - \cot(\frac{\pi \alpha_{\mathcal{P}}}{2})]$. The functions $g_i(t)$ are the hadronic form factors and $\beta_{\mathcal{P}}(t)$ is the Pomeron residue function, which gives the coupling of the Pomeron with the external particles.

Despite the initial success, traditional soft Pomeron amplitudes, which grow as a power of energy and lack transverse dynamics, face serious limitations at LHC and asymptotic energies. They violate unitarity constraints such as the Froissart bound, fail to account for multiple scattering effects, and cannot describe the impact-parameter structure or saturation phenomena observed experimentally. These shortcomings motivate the search for alternative formulations that incorporate nonlinear dynamics, unitarization mechanisms, and an explicit transverse space treatment.

2 Formulation in terms of an evolution equation

To better understand the high-energy behavior of elastic scattering amplitudes in impact parameter space (b -space), we analyze a simplified form of the soft Pomeron exchange. The phenomenological values of $\epsilon_{\mathcal{P}}$ and α' (in the GeV^{-2} scale) are typically small, and since we are interested in forward scattering where t is also small, it is reasonable to expand the signature factor in powers

of $\epsilon_{\mathcal{P}} + \alpha' t$. In particular,¹ we approximate

$$\cot \frac{\pi \alpha_{\mathcal{P}}(t)}{2} \sim -\frac{\pi}{2}(\epsilon_{\mathcal{P}} + \alpha' t) . \quad (6)$$

This simplifies the form of the amplitudes, avoiding trigonometric functions. Assuming the typical form factors and the residue function as pure exponential forms

$$g_i(t) = A_i e^{\beta_i t} \quad i = \{a, b\} , \quad (7)$$

and

$$\beta_{\mathcal{P}}(t) = \beta_0 e^{\beta_{\mathcal{P}} t} , \quad (8)$$

then, Eq.(5) can be analytically Fourier transformed to the impact parameter space:

$$\begin{aligned} \tilde{\mathcal{T}}(s, b) &= \frac{4\pi}{s} \int \frac{d^2 q_{\perp}}{2\pi} e^{-i \vec{q}_{\perp} \cdot \vec{b}_{\perp}} \mathcal{T}(s, -q^2) \\ &= \mathcal{A} s^{\epsilon_{\mathcal{P}}} \frac{e^{-b^2/4\mathcal{B}(s)}}{2\mathcal{B}(s)} \left[i + \frac{\pi}{2} \left(\epsilon_{\mathcal{P}} + \alpha' \frac{(b^2 - 4\mathcal{B}(s))}{4\mathcal{B}(s)^2} \right) \right] , \end{aligned} \quad (9)$$

where $\mathcal{A} = 4\pi A_a A_b \beta_0$ and $\mathcal{B}(s) = (\beta_a + \beta_b + \beta_{\mathcal{P}} + \alpha' \log s)$.

Re-defining $\tau = \log s$, after some algebra, we prove that Eq.(9) obeys exactly a diffusion equation with a linear term

$$(\partial_{\tau} - \alpha' \nabla_b^2 - \epsilon_{\mathcal{P}}) \tilde{\mathcal{T}}(\tau, b) = 0 , \quad (10)$$

where the Laplacian in 2-dimensions is

$$\nabla_b^2 = \partial_{bb} + \frac{1}{b} \partial_b . \quad (11)$$

The diffusion equation draws an analogy with the Schrödinger equation in imaginary time, with τ playing the role of the logarithm of the scattering energy (the rapidity).

However, the linear term $\epsilon_{\mathcal{P}} \tilde{\mathcal{T}}$ leads to power-law growth of amplitude, which ultimately violates both the Froissart bound [4] and the unitarity at asymptotic energies. That is, the simple-pole amplitude grows faster than it spreads in b -space. In a sense, at high energies the simple-pole Pomeron-like amplitude Eq.(5) is not appropriate to describe elastic scattering and must be replaced by something else. This behavior indicates that the linear evolution, although analytically tractable and phenomenologically useful at moderate energies, becomes insufficient to describe the dynamics at high energies where unitarity constraints become significant. To account for these effects and ensure a more realistic asymptotic behavior, it is natural to seek a nonlinear extension of Eq. (10) that

¹Noting that $\cot \left(\frac{\pi}{2} \alpha_{\mathcal{P}}(t) \right) = -\tan \left(\frac{\pi}{2} (\epsilon_{\mathcal{P}} + \alpha' t) \right)$

can tame the unbounded growth of the amplitude. Motivated by this physical picture, we propose the following nonlinear generalization:

$$\left[\partial_\tau - \alpha' \nabla_b^2 - \epsilon_{\mathcal{P}} \left(1 + i \frac{\lambda}{\epsilon_{\mathcal{P}}} \tilde{T} \right) \right] \tilde{T} = 0 , \quad (12)$$

and look for solutions of this equation. Separating it into the real and imaginary parts we arrive at a set of two coupled partial differential equations

$$\partial_\tau \tilde{T}_R = \alpha' \nabla_b^2 \tilde{T}_R + \epsilon_{\mathcal{P}} \left(1 - 2 \frac{\lambda}{\epsilon_{\mathcal{P}}} \tilde{T}_I \right) \tilde{T}_R , \quad (13)$$

$$\partial_\tau \tilde{T}_I = \alpha' \nabla_b^2 \tilde{T}_I + \epsilon_{\mathcal{P}} \left(1 - \frac{\lambda}{\epsilon_{\mathcal{P}}} \tilde{T}_I \right) \tilde{T}_I + \lambda \tilde{T}_R^2 . \quad (14)$$

We present the above complex evolution equation for scattering amplitudes in a recent work [9], based on Regge field theory, changing the standard approach in elastic scattering, turning it into an initial value problem.

The imaginary part Eq.(14) resembles the well-known Fisher-Komolgorov-Petrovsky-Piscunov equation (FKPP) [10,11] with an additional nonlinear term from the real part which usually is subdominant. Disregarding the quadratic term \tilde{T}_R^2 the imaginary part of the equation has some well-established properties, and under specific conditions it can be solved analytically [12]. This kind of equation was vastly explored in different scientific domains, biology, chemistry and physics. Recently, this equation has attracted interest in the high-energy physics community, since it maps the energy evolution described by an integro-differential equation for the gluon density [13]. The imaginary part resembles the Balitsky-Kovchegov (BK) equation [14–16] and the real part the Kovchegov-Szymanowski-Wallon (KSW) equation [17].

There is no justification for neglecting the quadratic term \tilde{T}_R^2 , which leads to a system of coupled partial differential equations. The initial conditions required to solve this system do not yield closed-form analytic solutions. In fact, analytic solutions are only possible under the assumption of a traveling wave with a specific speed, as shown in Ref. [12]. In our previous work [9], we began our analysis by using models defined in b -space as initial conditions for the evolution equation.

2.1 Closed-form solution in the diffusionless limit

The diffusion of elastic scattering in b -space, first discussed by Gribov [18], is related to Pomeron's slope α' from the linear trajectory, describing, together with the hadrons form factors, the shrinkage of the differential cross section. But diffusion was necessary for amplitudes like Eq.(5) i.e., a simple-pole Pomeron that violates unitarity, breaking then a building block of the Froissart theorem. Phenomenologically, from Eq. (12) we observe that the diffusion coefficient α' is compatible with zero, leading to a strong consequence in the interpretation

of the Pomeron's linear trajectory. The disappearance of this parameter is compensated by the presence of the nonlinear term and also has an influence on the Pomeron intercept $\epsilon_{\mathcal{P}}$, increasing its value, and more importantly, we obtain an ordinary first-order nonlinear differential equation

$$\left[\frac{\partial}{\partial \tau} - \epsilon_{\mathcal{P}} \left(1 + i \frac{\lambda}{\epsilon_{\mathcal{P}}} \tilde{T} \right) \right] \tilde{T} = 0 \quad (15)$$

with a complex analytic solution

$$\tilde{T}(\tau, b) = \frac{\tilde{T}_0(\tau_0, b)}{\left(1 + i \frac{\lambda}{\epsilon_{\mathcal{P}}} \tilde{T}_0(\tau_0, b) \right) e^{-\epsilon_{\mathcal{P}}(\tau - \tau_0)} - i \frac{\lambda}{\epsilon_{\mathcal{P}}} \tilde{T}_0(\tau_0, b)} , \quad (16)$$

where $\tilde{T}_0(\tau_0, b)$ is the b -profile at a given energy and τ_0 playing the role of initial value. In appendix A we show how to obtain Eq. (15) from RFT, where the Pomeron intercept $\epsilon_{\mathcal{P}}$ is interpreted as an effective mass and the nonlinear term λ is interpreted as the interaction coupling of the triple-Pomeron vertex.

To find the solution Eq.(16) we change the function $\tilde{T}(\tau, b)$ to $u(\tau, b) = 1/\tilde{T}(\tau, b)$ and the differential equation transforms into a linear relaxation equation

$$\left[\frac{\partial}{\partial \tau} + \epsilon_{\mathcal{P}} \right] u(\tau, b) = -i \lambda , \quad (17)$$

with the solution given by the sum of the homogeneous and the particular parts

$$u(\tau, b) = A(b) e^{-\epsilon_{\mathcal{P}} \tau} - i \frac{\lambda}{\epsilon_{\mathcal{P}}} \quad (18)$$

where $A(b)$ is an integration constant with respect to τ but with a b -dependence. The amplitude is then

$$\tilde{T}(\tau, b) = \frac{1}{A(b) e^{-\epsilon_{\mathcal{P}} \tau} - i \frac{\lambda}{\epsilon_{\mathcal{P}}}} . \quad (19)$$

Using $\tilde{T}(\tau_0, b) = \tilde{T}_0(b)$ as initial condition we obtain $A(b)$, and as a consequence the solution Eq.(16).

The logistic-type nonlinear evolution of the elastic amplitude in b -space can be mapped onto a dissipative (damped) system, where the nonlinear term functions as a regulator of the dynamics, ensuring unitarity, much like damping enforces equilibrium in mechanical systems. This invites an analogy with damped classical systems, such as RC circuits or overdamped harmonic oscillators, where damping plays the role of a mechanism that conducts the system toward equilibrium. In this dual representation, unitarization emerges either as nonlinear damping in \tilde{T} or as linear relaxation in u , providing both conceptual and computational insights into the dynamics of high-energy elastic scattering. This

analogy may also open the door to analyzing stability, fixed points, and relaxation times using tools from dynamical systems theory.

Equation (16) is remarkably simple and can quantitatively describe the experimental data from the ISR to the LHC energies (also the cosmic ray energies) using only two physical quantities. However, the values of the parameter ρ , which is represented by the ratio between the real and imaginary parts at $|t| = 0$, as coming from the experimental analysis are not sufficiently described and a reinterpretation of this quantity may be necessary. To account for a flexibility in the description of the real part of the amplitude we can simply promote ϵ_P to a complex effective mass $\tilde{\epsilon} = \epsilon_R + i\epsilon_I$

$$\left[\frac{\partial}{\partial \tau} - \tilde{\epsilon} \left(1 + i \frac{\lambda}{\tilde{\epsilon}} \tilde{T} \right) \right] \tilde{T} = 0 , \quad (20)$$

introducing one more parameter in the equation, holding the same analytic structure for the complex solution. It is interesting to express the real and imaginary parts of the differential equation to understand their behavior

$$\frac{\partial \tilde{T}_R}{\partial \tau} = \epsilon_R \left(1 - \frac{2\lambda}{\epsilon_R} \tilde{T}_I \right) \tilde{T}_R + \epsilon_I \tilde{T}_I \quad (21)$$

$$\frac{\partial \tilde{T}_I}{\partial \tau} = \epsilon_R \left(1 - \frac{\lambda}{\epsilon_R} \tilde{T}_I \right) \tilde{T}_I + \epsilon_I \left(1 - \frac{\lambda}{\epsilon_I} \tilde{T}_R \right) \tilde{T}_R . \quad (22)$$

Taking $\epsilon_I \rightarrow 0$ and $\lambda \tilde{T}_R^2 \rightarrow 0$, Eqs. (21) and (22) approximates to

$$\frac{\partial \tilde{T}_R}{\partial \tau} \simeq \epsilon_R \left(1 - \frac{2\lambda}{\epsilon_R} \tilde{T}_I \right) \tilde{T}_R \quad (23)$$

$$\frac{\partial \tilde{T}_I}{\partial \tau} \simeq \epsilon_R \left(1 - \frac{\lambda}{\epsilon_R} \tilde{T}_I \right) \tilde{T}_I , \quad (24)$$

respectively.

The evolution of the imaginary part of the amplitude in impact parameter space, \tilde{T}_I , follows a logistic growth pattern for a given initial profile. This behavior naturally emerges from the nonlinear term and reflects a saturation mechanism as energy increases. At low energies, the amplitude grows linearly with τ , passing by a region where nonlinear effects become significant, leading to a saturation of the amplitude.

The saturation effect can be interpreted in the language of Regge theory by associating \tilde{T}_I with the Pomeron density profile in b -space. As the energy increases, the Pomeron density also increases, until nonlinear interactions among Pomerons become important and lead to a limiting behavior, effectively "absorbing" Pomerons and saturating the density. In Fig. 1, we display the evolution of the imaginary part of the amplitude $\tilde{T}(\tau, b)$, which exhibits a logistic profile as

a function of the energy evolution variable τ . For any fixed value of the impact parameter b , the amplitude undergoes an initial linear growth at low τ , followed by a nonlinear transition region, and asymptotically approaches a saturation plateau dictated by the unitarity constraint.

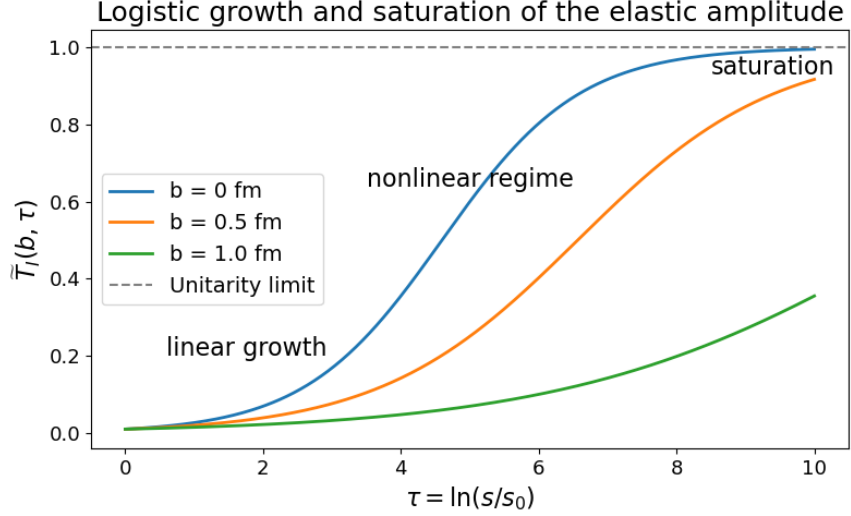


Figure 1: Evolution of the imaginary part of the elastic amplitude $\tilde{T}(\tau, b)$ at fixed impact parameter as a function of the energy evolution variable τ . The amplitude grows linearly at low energies, but saturates due to nonlinear effects, in analogy with gluon saturation in QCD. The plateau corresponds to the unitarity bound.

Such a mechanism resembles the gluon saturation phenomenon in QCD, as described by the nonlinear evolution equations such as BK [14–16] and B-JIMWLK [14, 19–26], where gluon recombination slows down the growth of the gluon distribution at large rapidity, when gluons carry small momentum fraction of the incident hadron (small- x physics). This connection is not entirely unexpected, as gluon saturation arises from ladder-type gluon interactions, precisely the building blocks of the QCD Pomeron [27]. In fact, it has been shown that the JIMWLK evolution can be reinterpreted as a Reggeon field theory in its own right, where Pomerons and their interactions emerge dynamically from QCD [28, 29].

An interesting aspect of Eq.(15) is the stability of the traveling wave due to the interplay between the nonlinear and the dispersive linear terms, behaving as a kink soliton solution. The two solutions are: ($\tilde{T} = 0$ unstable) and ($\tilde{T} = i \frac{\epsilon p}{\lambda}$ stable). Assuming a non zero initial condition T_0 , we can describe a kink soliton obtained from the solution Eq.(16) passing from $\tau = -\infty$ to $\tau \rightarrow \infty$. At asymptotic energies the amplitude is purely imaginary and the scattering is dominated by the inelastic processes. On the other hand, if we take the complex

parameter $\tilde{\epsilon}$ in Eq.(16) the asymptotic solution becomes

$$\lim_{\tau \rightarrow \infty} \tilde{T}(\tau, b) \rightarrow \frac{-\epsilon_I + i\epsilon_R}{\lambda} \quad (25)$$

and the real part of the elastic processes is still asymptotically preserved.

Note that the diffusion term is the main difference between the QCD evolution equations and the evolution equation (20). In perturbative QCD, for instance, the BK equation, mapped as FKPP equation, the diffusive term is usually attributed to the propagating front of the traveling wave. However, FKPP equation also presents the non-linear term.

To understand similarities and differences we compare a real logistic solution with FKPP type using a pure Gaussian as initial condition in both cases. For FKPP we set the diffusion coefficient to $\mathcal{D} = 0.1$. Of course, increasing this coefficient we increase the speed of the wave front. We show, that even without a diffusive term in logistic equation we still have a propagating wave front, due to the tail of the Gaussian provided as initial condition, with the advantage of having a analytic solution in closed form. The equations are:

$$\frac{\partial \mathcal{F}(x, t)}{\partial t} = \epsilon \left(1 - \frac{\lambda}{\epsilon} \mathcal{F}(x, t) \right) \mathcal{F}(x, t) \quad (26)$$

logistic equation with an analytic solution

$$\mathcal{F}(x, t) = \frac{\mathcal{F}_0(x) e^{\epsilon t}}{1 + \frac{\lambda}{\epsilon} \mathcal{F}_0(x) (e^{\epsilon t} - 1)} , \quad (27)$$

and the FKPP equation

$$\frac{\partial \mathcal{G}(x, t)}{\partial t} = \mathcal{D} \frac{\partial^2 \mathcal{G}(x, t)}{\partial x^2} + \epsilon \left(1 - \frac{\lambda}{\epsilon} \mathcal{G}(x, t) \right) \mathcal{G}(x, t) \quad (28)$$

solved numerically. The initial conditions are respectively:

$$\mathcal{F}_0(x) = \mathcal{F}(x, t_0) = A e^{-\frac{x^2}{\beta}} , \quad (29)$$

and

$$\mathcal{G}_0(x) = \mathcal{G}(x, t_0) = A e^{-\frac{x^2}{\beta}} . \quad (30)$$

The common parameters are : $\epsilon = 1$, $\lambda = 1$, $A = 0.01$, $\beta = 1$ and ($\mathcal{D} = 0.1$ exclusively for FKPP). In fig. 2 we compare the two equations using similar conditions. We plot the time evolution from 0 to 4 in equally spaced steps, where we see qualitatively the similar behavior.

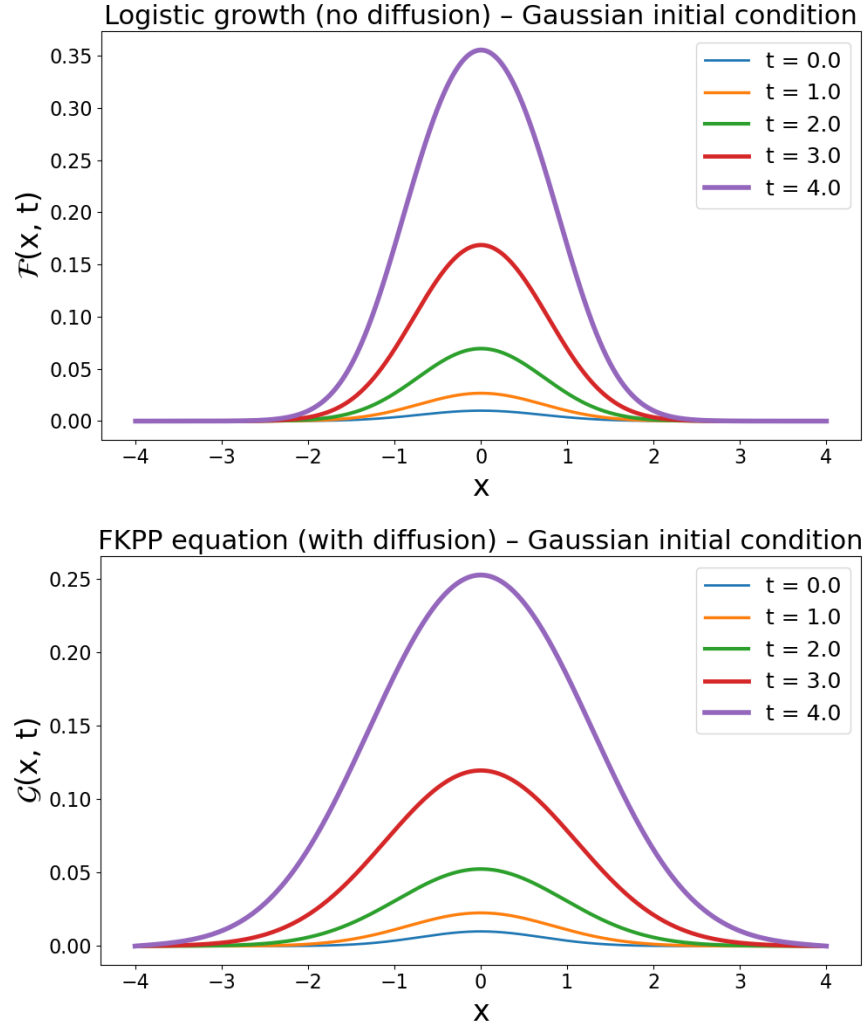


Figure 2: We compare pure logistic and FKPP solutions using a pure gaussian as initial condition. The upper panel shows the simple logistic equation without the diffusion term, whereas the lower shows the FKPP equation with the diffusion coefficient set to 0.1. Notice that the diffusive part spreads out the solution faster than the diffusionless part. Increasing the diffusion parameter increases the speed of the spread.

3 Mathematical properties and asymptotic theorems

In this section, we demonstrate that the proposed evolution equation satisfies the fundamental mathematical and asymptotic properties expected of high-energy scattering amplitudes. We show explicitly that the equation preserves unitarity, rigorously respects analyticity and the associated dispersion relations, and admits a unique, well-defined solution under physically motivated conditions. These rigorous results establish that the framework is not only phenomenologically motivated but also mathematically consistent with the key theorems that govern the high-energy regime of quantum field theory.

3.1 Unitarity

The unitarity condition states that the S-matrix $S(b) = 1 + i\tilde{T}(b)$ in b -space satisfies

$$S^*(b)S(b) = 1 , \quad (31)$$

which implies

$$(\tilde{T}_I(b) - 1)^2 + \tilde{T}_R^2(b) = 1 . \quad (32)$$

The above equality represents a circle in the $\tilde{T}_I(b) - \tilde{T}_R(b)$ complex plane centered at $(0, 1)$ with radius one.

The solutions for \tilde{T}_I are given by

$$\tilde{T}_{I\pm}(b) = 1 \pm \sqrt{1 - \tilde{T}_R^2(b)} . \quad (33)$$

It is easy to check that the "+" solution constrains

$$1 \leq \tilde{T}_I(b) \leq 2 \quad (34)$$

and the "-" solution

$$0 \leq \tilde{T}_I(b) \leq 1 . \quad (35)$$

We study the fixed points of Eq.(15) to understand whether the imaginary part of the amplitude satisfies unitarity. It has two possible solutions, $\tilde{T}_I^{(\min.)} = 0$ or $\tilde{T}_I^{(\max.)} = \frac{\epsilon_P}{\lambda}$. Numerically, the second solution could be greater than unity, thus, possibly crossing the two conditions (34) and (35) and thus, violation unitarity. In order to avoid such a violation, we can rescale the scattering amplitude to $\tilde{T}^{(r)} \rightarrow \frac{\lambda}{\epsilon_P} \tilde{T}$ and the new equation becomes

$$\left[\frac{\partial}{\partial \tau} - \epsilon_P \left(1 + i \tilde{T}^{(r)} \right) \right] \tilde{T}^{(r)} = 0 , \quad (36)$$

and the S-matrix is $S(b) = 1 + i\tilde{T}^{(r)}(b) = 1 + i\frac{\lambda}{\epsilon_P}\tilde{T}(b)$. As a consequence of the re-scaling the unitary condition of the "-" solution becomes

$$0 \leq \tilde{T}_I(b) \leq \frac{\epsilon_P}{\lambda} . \quad (37)$$

Note that the re-scaling of the scattering amplitude keeps Eq.(15) covariant, leading our amplitude unitarized for all b and τ values.

3.2 Froissart-Martin limit

Another key ingredient in hadronic scattering is the short-range behavior of strong interactions. Together with unitarity, these two ingredients allow to derive the Froissart theorem, establishing an upper bound for the asymptotic growth of the total cross section [4] leading to the bound

$$\sigma_{\text{tot.}}(\tau(s) \rightarrow \infty) \leq \mathcal{C} \tau^2 = \mathcal{C} \log^2 s . \quad (38)$$

From local and massive field theory Martin [5] proved that constant $\mathcal{C} = \frac{\pi}{m_\pi^2} \simeq 172$ mb where m_π is the pion mass.

From a theoretical perspective, the total cross section is determined by the extrapolation of the imaginary amplitude at the optical point. Up to now, Regge phenomenology was a successful approach to describe the energy dependence of the total elastic scattering of hadrons. In the seminal work from Donnachie-Landshoff, the Regge trajectories and the Pomeron trajectory were able to describe the hadronic scattering data in a broad energy range [30]. However, the positive power in the energy dependence due to the single-Pomeron intercept violates the Froissart bound. The unitarization of such a model was captured later by the introduction of a double Pomeron interaction.

We propose an evolution equation that, given a profile amplitude in b at a fixed energy, is able to describe all energy dependence of the scattering processes up to one physical quantity to be determined. To assess whether this evolution respects the Froissart-Martin bound we use the optical theorem and Fourier transform the imaginary part of the scattering amplitude from the b to the t space and we take the limit where $t \rightarrow 0$.

$$\sigma_{\text{tot.}}(\tau) = 2T_I(\tau, t=0) = 4\pi \int_0^\infty b db J_0(0) \tilde{T}_I(\tau, b) . \quad (39)$$

For specific forms of function $\tilde{T}_I(\tau, b)$ the equation above can be calculated in closed form. Geometrically, the interaction range is described by the imaginary profile in b -space given by the initial conditions, provided by models at fixed energy. In many models, the imaginary part of the scattering amplitude is one order of magnitude greater than the real part. For this reason, many authors simplify their models focusing only on the aspects of the imaginary amplitude. In general, the behavior of the profiles is smooth and decrease with increasing b . In what follows, to obtain an analytic solution for the total cross section, we

consider two extreme purely imaginary profiles: the Gaussian profile and the exponential one. The Gaussian profile is given by

$$T_0(\tau_0, b) = i B e^{-\beta b^2} \quad (40)$$

and, in this case, the amplitude in t space has an analytic solution and the total cross sections is given (the integral is calculated in appendix B.1)

$$\begin{aligned} \sigma_{\text{tot.}}^{\text{Gauss}}(\tau) &= 4\pi (\hbar c)^2 \int_0^\infty b db \frac{B e^{-\beta b^2}}{\left(1 - \frac{\lambda}{\epsilon_{\mathcal{P}}} B e^{-\beta b^2}\right) e^{-\epsilon_{\mathcal{P}}(\tau-\tau_0)} + \frac{\lambda}{\epsilon_{\mathcal{P}}} B e^{-\beta b^2}}, \\ &= 4\pi (\hbar c)^2 \frac{e^{\epsilon_{\mathcal{P}}(\tau-\tau_0)} \log\left(\frac{\epsilon_{\mathcal{P}} - B\lambda + B\lambda e^{\epsilon_{\mathcal{P}}(\tau-\tau_0)}}{\epsilon_{\mathcal{P}}}\right)}{2\beta\lambda(e^{\epsilon_{\mathcal{P}}(\tau-\tau_0)} - 1)}. \end{aligned} \quad (41)$$

For an exponential profile function

$$T_0(\tau_0, b) = i B' e^{-\beta' b}, \quad (42)$$

the total cross section is

$$\sigma_{\text{tot.}}^{\text{exp.}}(\tau) = 4\pi (\hbar c)^2 \frac{\epsilon_{\mathcal{P}} e^{\epsilon_{\mathcal{P}}(\tau-\tau_0)} \text{Li}_2\left(\frac{-B'(e^{\epsilon_{\mathcal{P}}(\tau-\tau_0)} - 1)\lambda}{\epsilon_{\mathcal{P}}}\right)}{\beta'^2 \lambda (e^{\epsilon_{\mathcal{P}}(\tau-\tau_0)} - 1)}. \quad (43)$$

For the Gaussian profile, the asymptotic limit when $\tau \rightarrow \infty$, is given by

$$\lim_{\tau \rightarrow \infty} \frac{\sigma_{\text{tot.}}^{\text{Gauss}}(\tau)}{\tau} = \frac{\epsilon_{\mathcal{P}}^2}{2\beta\lambda}, \quad (44)$$

showing that the total cross section will behave as simply as $\tau = \log s$ at asymptotic energies, whereas for the exponential profile we have

$$\lim_{\tau \rightarrow \infty} \frac{\sigma_{\text{tot.}}^{\text{exp.}}(\tau)}{\tau^2} = \frac{\epsilon_{\mathcal{P}}^3}{2\beta^2\lambda}, \quad (45)$$

which means that the total cross section behaves as ($\tau^2 = \log^2 s$). In the second case, the coefficient $\frac{\epsilon_{\mathcal{P}}^3}{2\beta^2\lambda} \ll \mathcal{C}$ for all the reasonable values of the parameters $\epsilon_{\mathcal{P}}$, β and λ , meaning that it satisfies Martin's bound coefficient.

This simple exercise shows that profiles with functional forms from Gaussian to exponential b , lead to the total cross sections that satisfy the Froissart-Martin limit, since Gaussian profiles fall much faster than exponential profiles with increasing b . As a conclusion, functions with b -dependence larger than exponential could lead to a violation of the Froissart bound, being considered long-range interactions.

3.3 Forward real amplitude

The real amplitude calculated at $t = 0$ together with the total cross section gives the parameter ρ . To analyze the possible range of the parameters we assume a

simplified model for the complex function $\tilde{T}_0(\tau_0, b)$ in order to calculate analytically the real amplitude and thus predict the possible values for ρ . As discussed in [31, 32] the real and imaginary parts cannot have the same t dependencies, but for the sake of simplicity we assume that at $t \simeq 0$ they could have the same dependencies.

As in the previous section, if the profile is a complex function with a Gaussian b -dependence

$$T_0(\tau_0, b) = (A + iB) e^{-\beta b^2} , \quad (46)$$

the Fourier transform of the real amplitude at $t = 0$ is

$$\begin{aligned} T_R(\tau, t=0) &= \int_0^\infty b db \tilde{T}_{0R}(\tau, b) \\ &= \frac{\epsilon_{\mathcal{P}} e^{\epsilon_{\mathcal{P}} \Delta \tau}}{4\beta\lambda(e^{\epsilon_{\mathcal{P}} \Delta \tau} - 1)} \left[\pi + 2 \tan^{-1} \left(\frac{\epsilon_{\mathcal{P}} - B\lambda + B\lambda e^{\epsilon_{\mathcal{P}} \Delta \tau}}{A\lambda(1 - e^{\epsilon_{\mathcal{P}} \Delta \tau})} \right) \right] . \end{aligned} \quad (47)$$

and the imaginary part is

$$\begin{aligned} T_I(\tau, t=0) &= \int_0^\infty b db \tilde{T}_{0I}(\tau, b) \\ &= \frac{\epsilon_{\mathcal{P}} e^{\epsilon_{\mathcal{P}} \Delta \tau}}{4\beta\lambda(e^{\epsilon_{\mathcal{P}} \Delta \tau} - 1)} \log \left[1 + \frac{2B\lambda}{\epsilon_{\mathcal{P}}} (e^{\epsilon_{\mathcal{P}} \Delta \tau} - 1) + (A^2 + B^2) \frac{\lambda^2}{\epsilon_{\mathcal{P}}^2} (e^{\epsilon_{\mathcal{P}} \Delta \tau} - 1)^2 \right] . \end{aligned} \quad (48)$$

The solution of the above integrals are give in appendix B.2. The ratio of the real and imaginary parts at the origin becomes ρ

$$\rho_{\text{gauss}}(\tau) = \frac{\pi + 2 \tan^{-1} \left(\frac{\epsilon_{\mathcal{P}} - B\lambda + B\lambda e^{\epsilon_{\mathcal{P}} \Delta \tau}}{A\lambda(1 - e^{\epsilon_{\mathcal{P}} \Delta \tau})} \right)}{\log \left[1 + \frac{2B\lambda}{\epsilon_{\mathcal{P}}} (e^{\epsilon_{\mathcal{P}} \Delta \tau} - 1) + (A^2 + B^2) \frac{\lambda^2}{\epsilon_{\mathcal{P}}^2} (e^{\epsilon_{\mathcal{P}} \Delta \tau} - 1)^2 \right]} \quad (49)$$

Taking the limit when τ goes to infinity

$$\lim_{\tau \rightarrow \infty} \rho_{\text{gauss}}(\tau) \rightarrow 0 . \quad (50)$$

From Eq.(50) it becomes clear that the energy dependence of ρ depends on the magnitude of the real and imaginary profiles as well as the parameters λ and $\epsilon_{\mathcal{P}}$. More realistic and physically acceptable profiles may keep similar properties.

3.4 Uniqueness

Equation (15) provides a unique solution for each different initial condition. To prove the uniqueness it is sufficient to prove that it is Lipschitz continuous, which is an essential condition for Picard–Lindelöf theorem which guarantees the existence of uniqueness. Let's recall Lipschitz theorem:

A function $f(z)$ is called *Lipschitz continuous* on a domain $\mathcal{D} \subset \mathbb{C}$ if there exists a constant $L > 0$ such that for all z_1 and $z_2 \in \mathbb{C}$ we have

$$|f(z_1) - f(z_2)| \leq L|z_1 - z_2| . \quad (51)$$

From Eq.(20) we can rewrite the differential equation as

$$\frac{\partial \tilde{T}}{\partial \tau}(\tau, b) = f(\tilde{T}(\tau, b)) , \quad (52)$$

where

$$f(\tilde{T}) = \epsilon_{\mathcal{P}}\tilde{T} + i\lambda\tilde{T}^2 , \quad (53)$$

with $f(\tilde{T})$ being our field of $\tilde{T} \equiv \tilde{T}(\tau, b)$.

Theorem: The function $f(\tilde{T})$ is Lipschitz continuous.

Proof: Let's take two point $f(\tilde{T}_1)$ and $f(\tilde{T}_2)$

$$\begin{aligned} f(\tilde{T}_1) - f(\tilde{T}_2) &= \epsilon_{\mathcal{P}}(\tilde{T}_1 - \tilde{T}_2) + i\lambda(\tilde{T}_1^2 - \tilde{T}_2^2) \\ &= \left(\epsilon_{\mathcal{P}} + i\lambda(\tilde{T}_1 + \tilde{T}_2) \right) (\tilde{T}_1 - \tilde{T}_2) \end{aligned} \quad (54)$$

As a consequence the norm of the above equation is

$$|f(\tilde{T}_1) - f(\tilde{T}_2)| = |\epsilon_{\mathcal{P}} + i\lambda(\tilde{T}_1 + \tilde{T}_2)| |\tilde{T}_1 - \tilde{T}_2| \quad (55)$$

and the triangular inequality gives

$$|f(\tilde{T}_1) - f(\tilde{T}_2)| \leq \left(|\epsilon_{\mathcal{P}}| + |\lambda| |\tilde{T}_1 + \tilde{T}_2| \right) |\tilde{T}_1 - \tilde{T}_2| . \quad (56)$$

Assuming \tilde{T}_1 and \tilde{T}_2 inside a bounded set $|\tilde{T}_1|, |\tilde{T}_2| \leq M$, we have $|\tilde{T}_1 + \tilde{T}_2| \leq 2M$ that implies

$$|f(\tilde{T}_1) - f(\tilde{T}_2)| \leq \left(|\epsilon_{\mathcal{P}}| + 2|\lambda| M \right) |\tilde{T}_1 - \tilde{T}_2| , \quad (57)$$

where $L = |\epsilon_{\mathcal{P}}| + 2|\lambda| M$. We thus prove that

$$|f(\tilde{T}_1) - f(\tilde{T}_2)| \leq L |\tilde{T}_1 - \tilde{T}_2| \quad (58)$$

and the function f is Lipschitz continuous. Since the vector field $f(\tilde{T}) = \epsilon_{\mathcal{P}}\tilde{T} + i\lambda\tilde{T}^2$ is continuous and locally Lipschitz continuous on \mathbb{C} , the Cauchy-Lipschitz (Picard-Lindelöf) theorem applies. Therefore, for any given initial condition $\tilde{T}(\tau_0, b) = \tilde{T}_0(b)$, there exists a unique solution $\tilde{T}(\tau, b)$ to the differential equation in a neighborhood of τ_0 . In addition, because the vector field has polynomial growth and no singularities, the solution can be extended globally for all values of τ .

However, if we reach an infinity value of τ it is impossible to return back to smaller values of τ without passing by singularities. This phenomenon means that the saturation state $\lim_{\tau \rightarrow \infty} \tilde{T}(\tau, b) \rightarrow i\epsilon_{\mathcal{P}}/\lambda$ is a terminal attractor of the system, characterizing a physical limit of the evolution of the amplitude with respect to the energy. In fig.3 we show several solutions $\tilde{T}(\tau, b)$, running with the variable τ , corresponding to different complex initial conditions, leading to the saturated value $i\epsilon_{\mathcal{P}}/\lambda$. This property unveils the universality of the saturation behavior in high energy independent of the initial fluctuations.

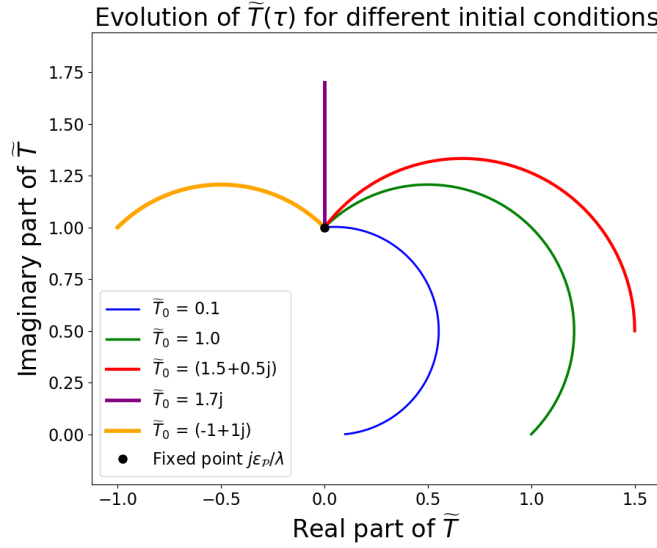


Figure 3: The figure shows several solutions $\tilde{T}(\tau)$ corresponding to different complex initial conditions. The curves describes the τ evolution. Despite the divergent initial trajectories as initial conditions in the complex plane, all the solutions converge asymptotically to the same value $i\epsilon_{\mathcal{P}}/\lambda$. We chose the parameters: $\epsilon_{\mathcal{P}} = 0.1$, $\lambda = 0.1$ and $\tau_0 = 1$.

3.5 Dispersion relations

In high energy physics, the analytic structure of the amplitudes for elastic scattering is fundamental to comprehend the properties of strong interactions. Causality, governed by Kramers-Krönig relations (dispersion relations), imposes strict conditions on analyticity of the theory. Here we analyze these properties for the amplitude $\tilde{T}(\tau, b)$ fixed b varing $\tau = \log s$.

From the general solution of the complex logistic equation Eq.(16)

$$\tilde{T}(\tau, b) = \frac{\tilde{T}_0(\tau_0, b)}{\left(1 + i \frac{\lambda}{\epsilon_{\mathcal{P}}} \tilde{T}_0(\tau_0, b)\right) e^{-\epsilon_{\mathcal{P}}(\tau - \tau_0)} - i \frac{\lambda}{\epsilon_{\mathcal{P}}} \tilde{T}_0(\tau_0, b)}, \quad (59)$$

if $\tilde{T}_0(\tau_0, b)$ is an arbitrary complex function, we should analyze the existence of poles, searching for singularities. The denominator is given by

$$D(\tau) = \left(1 + i \frac{\lambda}{\epsilon_{\mathcal{P}}} \tilde{T}_0(\tau_0, b)\right) e^{-\epsilon_{\mathcal{P}}(\tau - \tau_0)} - i \frac{\lambda}{\epsilon_{\mathcal{P}}} \tilde{T}_0(\tau_0, b). \quad (60)$$

To be a singular solution we need $D(\tau) = 0$, that implies

$$\left(1 + i \frac{\lambda}{\epsilon_{\mathcal{P}}} \tilde{T}_0(\tau_0, b)\right) e^{-\epsilon_{\mathcal{P}}(\tau - \tau_0)} = i \frac{\lambda}{\epsilon_{\mathcal{P}}} \tilde{T}_0(\tau_0, b). \quad (61)$$

We decompose the function $\tilde{T}_0(\tau_0, b)$ in terms of its real and imaginary parts

$$\tilde{T}_0(\tau_0, b) = \tilde{T}_{0R} + i\tilde{T}_{0I}. \quad (62)$$

The denominator Eq.(60) becomes

$$\left(1 - \frac{\lambda}{\epsilon_{\mathcal{P}}} \tilde{T}_{0I} + i \frac{\lambda}{\epsilon_{\mathcal{P}}} \tilde{T}_{0R}\right) e^{-\epsilon_{\mathcal{P}}(\tau - \tau_0)} = i \frac{\lambda}{\epsilon_{\mathcal{P}}} (\tilde{T}_{0R} + i\tilde{T}_{0I}), \quad (63)$$

and we obtain two separate equations for the real and imaginary parts

$$\left(1 - \frac{\lambda}{\epsilon_{\mathcal{P}}} \tilde{T}_{0I}\right) e^{-\epsilon_{\mathcal{P}}(\tau - \tau_0)} = -\frac{\lambda}{\epsilon_{\mathcal{P}}} \tilde{T}_{0I}, \quad (64)$$

$$\frac{\lambda}{\epsilon_{\mathcal{P}}} \tilde{T}_{0R} e^{-\epsilon_{\mathcal{P}}(\tau - \tau_0)} = \frac{\lambda}{\epsilon_{\mathcal{P}}} \tilde{T}_{0R}. \quad (65)$$

If $\tilde{T}_{0R} \neq 0$, Eq. (65) imposes

$$e^{-\epsilon_{\mathcal{P}}(\tau - \tau_0)} = 1, \quad (66)$$

which is possible only² in the case $\tau = \tau_0$, implying that Eq.(64) can never be satisfied and no singularity appears for $\tau > \tau_0$. On the other hand, if $\tilde{T}_{0R} = 0$, we obtain

$$\left(1 - \frac{\lambda}{\epsilon_{\mathcal{P}}} \tilde{T}_{0I}\right) e^{-\epsilon_{\mathcal{P}}(\tau - \tau_0)} = -\frac{\lambda}{\epsilon_{\mathcal{P}}} \tilde{T}_{0I}. \quad (67)$$

This condition could only be satisfied if $\tilde{T}_{0I} = 0$ and $\tau \rightarrow \infty$ or for an specific complex value of τ . However, as long as \tilde{T}_{0I} is bounded, which is the case by the unitarity constraints, and $\lambda, \epsilon_{\mathcal{P}} > 0$, this equation cannot lead to a real τ , meaning that the only possibility that the denominator diverges is for complex τ .

On the other hand, causality in strong interaction imposes that the scattering amplitude cannot contain information coming from a past time. This translates by the analyticity condition over $\tilde{T}(s, b)$, where the energy s is related to the

²Of course we disregard $\epsilon_{\mathcal{P}} = 0$ since this is a trivial solution.

time by the Fourier transform. To ensure causality, $\tilde{T}(s, b)$ must be analytic in the superior semi-plane of the complex s

$$\text{Im}(s) > 0 \quad \Rightarrow \quad \tilde{T}(s, b) \quad \text{analytic} \quad (68)$$

In terms of $\tau = \log s$, this implies that $\tilde{T}(\tau, b)$ is analytic for

$$\text{Im}(\tau) > 0. \quad (69)$$

The analyticity condition $\text{Im}(s) > 0$ allows us to apply dispersion relations

$$\text{Re} \tilde{T}(s, b) = \frac{1}{\pi} \mathcal{P} \int_{-\infty}^{+\infty} \frac{\text{Im} \tilde{T}(s', b)}{s' - s} ds'. \quad (70)$$

A formal test of analyticity consists in verifying Cauchy-Riemann derivatives. In this case, assuming a complex evolution variable $\tau = \tau_R + i\tau_I$, taking the real and imaginary parts $\text{Re} \tilde{T}(\tau_R, \tau_I)$ and $\text{Im} \tilde{T}(\tau_R, \tau_I)$ respectively, it is trivial to prove that

$$\frac{\partial \text{Re} \tilde{T}(\tau_R, \tau_I)}{\partial \tau_I} = \frac{\partial \text{Im} \tilde{T}(\tau_R, \tau_I)}{\partial \tau_R} \quad (71)$$

and

$$\frac{\partial \text{Re} \tilde{T}(\tau_R, \tau_I)}{\partial \tau_R} = - \frac{\partial \text{Im} \tilde{T}(\tau_R, \tau_I)}{\partial \tau_I} \quad (72)$$

satisfy Cauchy-Riemann conditions. We leave the prove to the interested reader.

It is nonetheless important to remember that in high-energy physics the Kramers-Krönig relations are applied in momentum space precisely at $t = 0$. But since we have shown that $T(\tau, b)$ is analytic and well defined in τ and b , dropping to zero in between a Gaussian and an exponential decay it implies that $T(s, t)$ will inherit the analytic properties from b -space. So, its Fourier transform will have no singularities and will also be analytic. The typical monotonic decreasing profiles for the real and imaginary parts of $\tilde{T}(\tau, b)$ will ensure the convergence of the Fourier transform to the t -space.

The principles of analyticity and causality are fundamental principles imposing strict constraints on the evolution of the scattering amplitudes. Our equation respects these constraints, ensuring that our solution is physically coherent and mathematically well defined.

4 Analysis of our results

Although the present work focuses on the theoretical structure of the complex non-linear evolution equation, its application to phenomenological models is promising. As an evolution equation our solution requires a complex b -profile in a fixed energy, $\tilde{T}_0(\tau_0, b)$, to evolve the scattering process along rapidity. In

this section we briefly describe our results in the Fourier-transformed space in two regimes: the full t -range (corresponding to full b -profiles) and the forward scattering (corresponding to large b -profiles). Realistic b -space profiles extracted from elastic scattering data can serve as initial conditions for a broad t -range. Some examples:

- Kohara-Ferreira-Kodama (KFK) model [33] — based on the stochastic vacuum model [34] uses asymptotic forms of Wilson loop correlators to describe the scattering amplitudes.
- Bourrely-Soffer-Wu (BSW) model [35] — an eikonalized model inspired in the crossing symmetry of s and u Mandelstam variables from field theories.
- Donnachie-Landshoff (DL) model [36] — based on single-Pomeron exchange plus double-Pomeron exchange (to account for unitarity) in the t channel in the Regge formalism.
- Białas-Bzdak model (BB) [37] — based on the modelization of the proton as a pair of quark and di-quark, distributed according to a Gaussian probability density. The model evokes Glauber techniques to superpose the interactions. The model was extended by Csörgő and Nemes to account the real part of the amplitude [38,39]. This is the so-called RealBB model.

Our preliminary studies show that the evolution of full t -profiles captures the main features of the energy dependence of the total cross section and elastic differential cross section. To capture the Coulomb interference details we use forward amplitudes based on data-driven models. A detailed phenomenological analysis, including fitting procedures and predictions for LHC energies and beyond, will be presented in a forthcoming publication.

The models above discussed can be represented in b -space, where the real and imaginary parts of their amplitudes can be decoupled to be injected into our equation. The four models described in full t -range, have both the b and s dependencies, albeit for our purposes we take each of these models at a single energy, where it has a good match with a specific experimental dataset. The similarities between the four models lie in the behavior of the amplitudes. In momentum space, the real parts fall to zero faster than the imaginary part, crossing zero according to Martin's theorem [40], becoming negative and then reducing again to zero, whereas the imaginary parts fall to zero later constraining the position of the dip. The interplay between real and imaginary parts around the dip gives its magnitude.

The model for the forward scattering is based on exponential forms in t for real and imaginary amplitudes with a linear t -term to account for the passage of the real amplitude through zero. This model was described in our previous works [31,32] with its extension to account the energy dependence [41] and the analytical connection between real and imaginary parts. This model describes accurately the behavior of the real amplitude in the forward regime up to $t \simeq 0.2 \text{ GeV}^2$.

To determine the physical quantities λ and $\tilde{\epsilon}$ adequate for each model, we use the real $\tilde{T}_{0R}(b)$ and imaginary $\tilde{T}_{0I}(b)$ profiles in a given energy from a specific model and we fit our solution in a different energy. To avoid bias, we usually take a large energy gap, for instance, if we give as an input an ISR energy we fit a LHC energy where the distributions were measured in a broad momentum range. Of course different methods of fitting would be possible, but we chose the simplest χ^2 method. The differential cross section is written as the absolute square of our evolution equation given by the solution of Eq.(20)

$$\tilde{T}(\tau, b) = \frac{\tilde{T}_0(\tau_0, b)}{\left(1 + i \frac{\lambda}{\tilde{\epsilon}} \tilde{T}_0(\tau_0, b)\right) e^{-\tilde{\epsilon}(\tau - \tau_0)} - i \frac{\lambda}{\tilde{\epsilon}} \tilde{T}_0(\tau_0, b)}, \quad (73)$$

with a complex $\tilde{\epsilon}$. We anticipate that for long t we consider $\epsilon_I = 0$, since this quantity is relevant only in the very forward scattering where the real amplitude can be determined with accuracy. Since the long- t models are aimed to describe the global structure of the data they are more insensitive to ϵ_I . In the very forward scattering this parameter shows to be relevant to describe the values of ρ .

4.1 t -dependence of elastic scattering: forward and large- $|t|$ behavior

To give the reader an idea of the quality of our description we present a few representative numerical results.

To determine the coupling and the effective mass of our equation we fit the differential cross section data at a given energy and constraint the effective real mass ϵ_R with the fit of Eq.(39) for the four models. The physical parameters are given in table 1. For full- t models, the imaginary contribution of the mass ϵ_I seems to be insensitive and we set it to zero. For the forward model used as initial condition, ϵ_I becomes sensitive and adjusts the real part. As show in table 1 the effective mass and coupling are equal for the forward model, leading to further simplification to the evolution equation. In this case the unitarity bound would be exactly the unit and the unitary re-scaled condition given in Eq.(37) would recover the standard condition.

	ϵ_R	λ	ϵ_I
KFK	0.122	0.088	-
BSW	0.124	0.092	-
DL	0.128	0.103	-
RealBB	0.135	0.095	-
Forward	0.15	0.15	0.014

Table 1: The parameters ϵ_R , ϵ_I and λ are presented separately for KFK, BSW, DL, RealBB and the Forward models used as initial conditions.

In figure 4 we show our preliminary results for the differential cross section using as an example KFK model as initial condition. We observe that the structure of the dip and bump are naturally reproduced by the evolution equation from ISR to LHC energies. The other models give similar description with local changes in different t regions, reflecting the differences from the initial conditions.

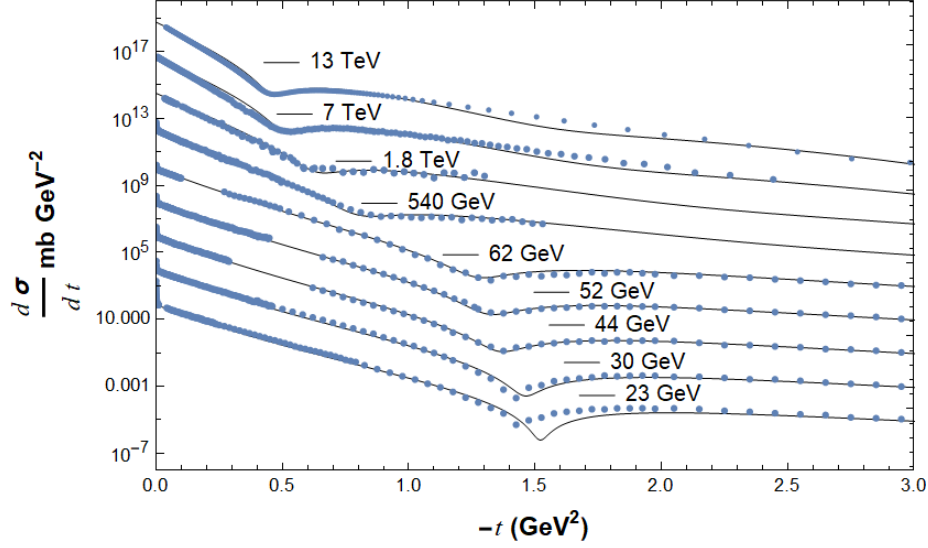


Figure 4: Description for the differential cross section data from ISR to LHC energies using KFK model as initial condition, mixing the pp and $p\bar{p}$ data. Notice that the passage from pp to $p\bar{p}$ seems to be a natural energy evolutionary process, disregarding the crossing symmetry processes.

In fig.5 we show our results for the differential cross sections in the range ($0 < |t| < 0.2 \text{ GeV}^2$) for the forward profile given as IC at 52.8 GeV. In this figure we add the Coulomb amplitude to the real part. In fig.6 we show the real part of the forward amplitude coming from our evolution equation at 13 TeV as an example and we compare it with the Coulomb amplitude, given by the electromagnetic interaction of the charged hadrons. We observe that the real part of the amplitude crosses zero twice. The first zero arises from the interference with the Coulomb amplitude, which is negative in the case of pp scattering. The second zero, known as the Martin zero, originates purely from the nuclear interaction. Qualitatively, the behavior of the amplitude in the very forward region resembles that of the large- t models; however, in those models, the Martin zero typically appears at larger values of $|t|$, shifted further to the right in momentum transfer.

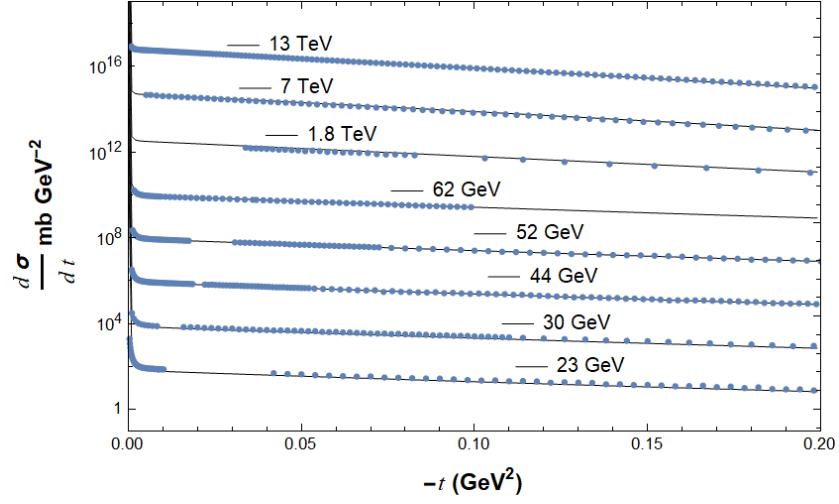


Figure 5: Differential cross sections in the forward region ($0 < |t| < 0.2 \text{ GeV}^2$), obtained from the evolved forward scattering profile with initial conditions at 52.8 GeV. The real part of the amplitude includes the Coulomb contribution.

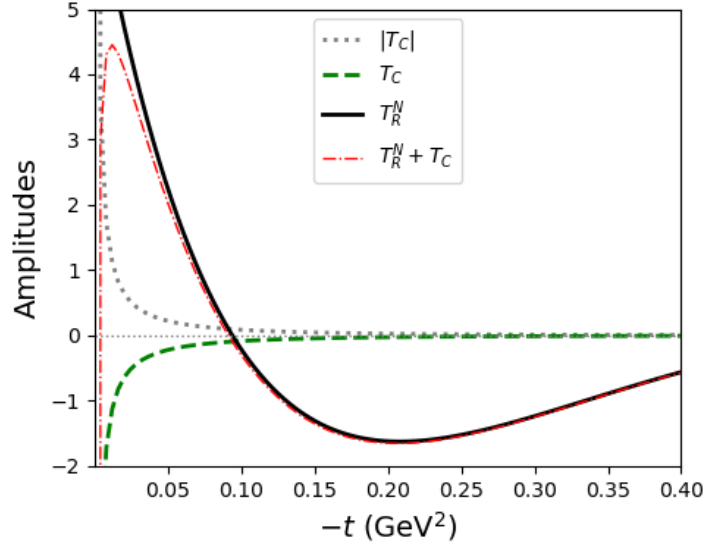


Figure 6: The real nuclear amplitude at 13 TeV with the Coulomb part. The dashed-dotted line represent the sum $T_R^N + T_C$, solid line is T_R^N and the dotted line is the Coulomb amplitude. Note that the nuclear and Coulomb amplitudes interplays creating two zeros near the origin. The first zero is the pure compensation of the nuclear part with the imaginary negative Coulomb interaction and the second zero is the so called Martin's zero.

4.2 Total cross section $\sigma_{\text{tot.}}$

The imaginary part of Eq.(73) into Eq.(39) determines the total cross section up to two physical quantities: $\tilde{\epsilon}$ and λ . We notice that the total cross section is mainly influenced by the effective real mass ϵ_R , while the other quantities do not affect qualitatively the energy dependence of $\sigma_{\text{tot.}}$. For large- t models as initial conditions the effective real mass is $\epsilon_R \sim 0.12$, describing accurately the experimental data from ISR to LHC energies and being extrapolated to the very high energy cosmic rays. In fig.(7) we represent our solution using the KFK model as an example to describe the total cross section data. The other models lead to similar description.

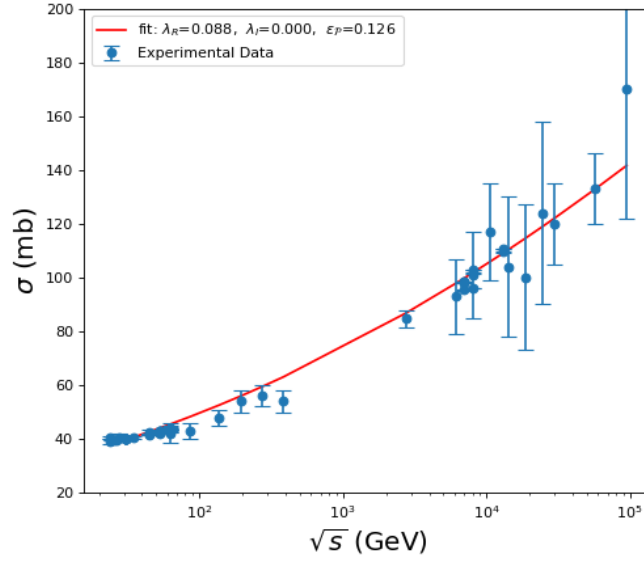


Figure 7: Fit of the experimental data from PDG (COMPETE) compilation [42] from ISR to cosmic ray energies.

4.3 The ratio ρ

The ratio ρ is a physical parameter determined at the origin. In most of the experimental analyses, this quantity comes from simplified exponential forms where the real and imaginary amplitudes have the same t dependence. It is important to stress that this procedure of extracting ρ is already an assumption and as a consequence it is model dependent.

The dispersion relations connect the real and imaginary parts of amplitudes. Since the total cross section is given by the pure imaginary part at the origin, its behavior, up to asymptotic energies could give us the value of the parameter

ρ . Many studies have been conducted to predict ρ from the parametrization of the total cross section [42–46]. It is important to stress that in order to calculate ρ from dispersion relations we need the knowledge of the entire σ_{tot} , which for very high energies may be not realistic. Extrapolations are always used and dispersion relations are not universal in this sense. Since our equation connects analytically the real and the imaginary parts in the entire s domain, the dispersion relations constraints are automatically satisfied.

For the long- t initial conditions we observe that ρ is almost constant in a broad energy range with an asymptotic decreasing trend and from Eq.(25) when $\tau \rightarrow \infty$ and $\epsilon_I = 0$ the amplitude is pure imaginary and $\rho \rightarrow 0$. However, for forward scattering initial conditions, which is based on a data-driven model, the trend of ρ approaches the experimental behavior and the imaginary part of the effective mass ϵ_I plays an important role.

Our conclusion is that ρ should not be treated as an experimental value since it is hidden behind the imaginary part, which is ten times larger than the real part at the origin, and a slightly change in the parametrization of the amplitudes could lead to strong modifications in the numerical values.

As signalized before, other interesting interference effects on the real part could be potentially observed at LHC energies [47,48], constraining the behavior of the real amplitude showing a clear interference pattern. If this is the case, as a natural consequence, the values of ρ would be more realistic.

4.4 Crossing symmetry

It is noteworthy that our evolution equation naturally reproduces the features observed in the experimental $p\bar{p}$ data at 540 GeV and 1800 GeV, starting from initial conditions fitted to ISR pp data, as shown in Fig. 4. In particular, the equation predicts the emergence of a shallower dip structure at intermediate energies, such as 540 and 1800 GeV, followed by the reappearance of a sharper dip at LHC energies. This suggests that the apparent differences between pp and $p\bar{p}$ differential cross sections at these energies may be a natural consequence of the non-linear evolution.

The ability of our model to smoothly evolve the amplitude from ISR pp energies through the Tevatron $p\bar{p}$ region, while maintaining consistency with available data, hints at a deeper universality in the scattering dynamics at high energies. A more rigorous test of this hypothesis would involve reconstructing both pp and $p\bar{p}$ amplitudes at ISR energies using a data-driven model and evolving them separately to higher energies, allowing for a direct comparison of the predicted and observed differences.

5 Comments and Conclusions

In this work, we derive a universal evolution equation for elastic scattering of hadrons, rooted in RFT and structurally similar to QCD small- x evolution

equations. This approach captures the essential saturation dynamics of the scattering amplitude through a non-linear evolution process.

Our formalism reveals that the unitarity constraint naturally emerges from a logistic-type mechanism in rapidity space. Unlike traditional perturbative QCD approaches that rely heavily on transverse diffusion, we demonstrate that in the elastic regime, the diffusive term becomes redundant. Its role is effectively taken over by the intrinsic non-linearity of the strong interaction. As a result, our formalism respects key high-energy constraints, including unitarity, the Froissart bound, and dispersion relations.

Although the evolution equation is formally local in the impact parameter b , as the underlying Regge-inspired Lagrangian includes rapidity ($\tau = \log s$) derivatives but no spatial gradients, the structure of the amplitude $\tilde{T}(\tau, b)$ reflects a non-trivial interplay between its linear and nonlinear components, both explicitly dependent on b . This dependence effectively couples different regions in b -space through their shared evolution dynamics, inducing an emergent non-locality. As a result, the amplitude evolves towards a saturation regime where each b -dependent component asymptotically approaches the unitarity (black disk) limit, but the full profile retains a spatially correlated structure.

Importantly, we find that the real part of the Pomeron mass (Pomeron intercept) governs the total cross section, while the non-linear coupling λ controls the energy evolution of dip and bump structures in the differential cross section. Our results naturally explain the transition from pronounced dips at ISR energies to shallower structures at higher energies, such as in $p\bar{p}$ scattering at 540 and 1800 GeV.

Regarding the forward scattering regime, we argue that the ρ parameter (the ratio of real to imaginary parts at $t = 0$) should not be treated as a direct observable. Instead, it is more robust to analyze features of the differential cross section that signal nontrivial interference between real and imaginary parts. The existence of such structures can place meaningful constraints on the real part of the amplitude, providing a more solid foundation for modeling initial conditions.

The logistic equation used here dynamically saturates the amplitude, preventing indefinite growth with energy. This can be interpreted as a signal of confinement at the level of interaction strength: the non-linear term effectively localizes the amplitude in impact parameter space, reflecting the inability of color fields to spread freely at large distances, a hallmark of QCD confinement.

Finally, the evolution equation admits a natural interpretation within the framework of dynamical systems theory. The nonlinear saturation term, analogous to a damping force, ensures the system's convergence toward a finite asymptotic amplitude, respecting unitarity. The equation features two fixed points: a trivial one at zero amplitude and a non-trivial saturated solution, proportional to $i\epsilon_P/\lambda$, which represents the unitarity limit. A linear stability analysis reveals that the zero-amplitude fixed point is unstable, while the saturated state is stable, confirming that the system dynamically evolves toward saturation. This behavior mirrors classical damped systems, where dissipation drives the system to equilibrium. Moreover, the structure of the equation aligns

with reaction-diffusion models such as FKPP, suggesting that elastic scattering evolution may belong to a broader universality class of nonlinear systems characterized by saturation and wavefront propagation. These dynamical features strengthen the robustness and predictive power of our framework, offering a physically transparent mechanism for unitarization.

A Deriving the evolution equation

Regge field theory (RFT) extends Regge phenomenology into the realm of quantum field theories treating Reggeons as quantum fields. Its origins started with Gribov in his seminal work of Reggeon Calculus [49], where he introduced for the first time hybrid Feynman diagrams for Pomeron fields. It combines the complex angular momentum analysis of Regge phenomenology with the principles of field theory. At high energies, the Pomeron is the dominant reggeon and its fields are the building blocks for a Lagrangian. In what follows we are inspired in the work from Alessandrini-Amati-Ciafaloni [50]. The starting point is the RFT Lagrangian density in $2 + 1$ proposed in the 1970's [51–53]

$$\mathcal{L} = -\frac{1}{2}\bar{\Psi}\overleftrightarrow{\partial}_\tau\Psi - \alpha'\nabla_b\bar{\Psi}\cdot\nabla_b\Psi + \epsilon_{\mathcal{P}}\bar{\Psi}\Psi - i\lambda\bar{\Psi}(\Psi + \bar{\Psi})\Psi. \quad (74)$$

This Lagrangian follows some restrictions from the hybrid Feynman rules of RFT. For instance, the interaction term must have a negative sign due to the exchange of a single Pomeron and the vertex of the interaction, which is pure imaginary [51]. However, we are not interested in calculating the Pomeron propagator or the renormalization aspects of the theory. We are interested in finding stable solutions to our evolution equation for elastic scattering. In this sense we allow a violation of the negative sign for the interaction term at the Lagrangian level. Another modification is the suppression of the kinetic term (diffusion part), since as was shown, the kinetic part is compensated by the non-linear term, making the diffusion a redundant contribution and worst, creating some non-natural oscillations in the Fourier transformed amplitude. Retaining the kinetic term would simply reintroduce diffusion into the evolution equation for the scattering amplitudes. In terms of a Lagrangian the absence of the kinetic part might bring some strong theoretical consequences, since the lack of a kinetic term leads to non-propagating fields and the system is governed entirely by the potential, leading to non-dynamical solutions. We thus write our effective Lagrangian in $0 + 1$,

$$\mathcal{L}_{\text{eff.}} = -\frac{1}{2}\bar{\Psi}\overleftrightarrow{\partial}_\tau\Psi + \epsilon_{\mathcal{P}}\bar{\Psi}\Psi + i\lambda\bar{\Psi}(\Psi + \bar{\Psi})\Psi, \quad (75)$$

with the Pomeron field Ψ and its conjugate $\bar{\Psi}$. The imaginary time $\tau = i t$ plays the role of the logarithm of the energy, $\epsilon_{\mathcal{P}}$ is the Pomeron intercept (mass) and λ is the triple Pomeron coupling. In order to avoid working with an imaginary coupling the Pomeron fields are re-scaled and the Lagrangian becomes purely

real

$$\mathcal{L}_{\text{eff.}} = \frac{1}{2} q \overleftrightarrow{\partial}_\tau p - \epsilon_{\mathcal{P}} q p - \lambda q (p + q) p, \quad (76)$$

where the fields q and p are related to Gribov's Pomeron fields, $q = i\bar{\Psi}$, $p = i\Psi$ depending on b and τ . The Lagrangian density (76) gives rise to the Hamiltonian density

$$\mathcal{H} = \sum_i \pi_i \dot{Q}_i - \mathcal{L}_{\text{eff.}}, \quad (77)$$

with

$$\pi_i = \frac{\partial \mathcal{L}_{\text{eff.}}}{\partial \dot{Q}_i} \quad (78)$$

and Q_i the fields q and p . The Hamiltonian is related to the Hamiltonian density by

$$H(\tau) = \int d^2\vec{b} \mathcal{H}(\vec{b}; \tau) = \int d^2\vec{b} \left(\epsilon_{\mathcal{P}} q p + \lambda q (p + q) p \right). \quad (79)$$

From the canonical quantization the fields q and p are promoted to creation and annihilation operators, respectively, following the commutation relation

$$[\hat{p}(\vec{b}, \tau), \hat{q}(\vec{b}', \tau)] = -\delta^{(2)}(\vec{b} - \vec{b}'), \quad (80)$$

where the sign -1 is due to the imaginary triple-Pomeron coupling. The imaginary time Schrödinger equation is thus

$$\frac{\partial}{\partial \tau} |\psi\rangle = -H |\psi\rangle, \quad (81)$$

where the most general state vector can be expanded using an infinite set of correlation functions $G_k(\vec{b}_1, \dots, \vec{b}_k; \tau)$ in terms of a generalized coherent state

$$|\psi(\tau)\rangle = e^{-\hat{M}(\tau)} |\psi(0)\rangle \quad (82)$$

where the evolution operator $\hat{M}(\tau)$ is

$$\hat{M}(\tau) = \sum_{k=1}^{\infty} \frac{1}{k!} \int d^2\vec{b}_1 \dots d^2\vec{b}_k \hat{q}(\vec{b}_1) \dots \hat{q}(\vec{b}_k) G_k(\vec{b}_1, \dots, \vec{b}_k; \tau), \quad (83)$$

and $|\psi(0)\rangle$ is the perturbative vacuum state of the theory such that

$$\hat{p}(\vec{b}_k) |\psi(0)\rangle = 0 \quad (84)$$

for any k . Note that the n-point correlation function is

$$G_k(\vec{b}_1, \dots, \vec{b}_k; \tau) = \langle \psi(0) | \mathcal{T} \left\{ q(\vec{x}_1) \dots q(\vec{x}_k) p(\vec{y}_1) \dots p(\vec{y}_k) \right\} | \psi(0) \rangle, \quad (85)$$

where the impact parameter is defined as $\vec{b}_k = \vec{x}_k - \vec{y}_k$.

Expanding Eq.(82) we obtain

$$\begin{aligned}
|\psi(\tau)\rangle &= \left(1 - \hat{M}(\tau) + \frac{1}{2!}\hat{M}^2(\tau) - \frac{1}{3!}\hat{M}^3(\tau)\dots\right)|\psi(0)\rangle \\
&= \left\{1 - \left(\int_b \hat{q}(\vec{b}) G_1(\vec{b}; \tau) + \frac{1}{2!} \int_{b_1, b_2} \hat{q}(\vec{b}_1) \hat{q}(\vec{b}_2) G_2(\vec{b}_1, \vec{b}_2; \tau) + \dots\right) + \right. \\
&\quad + \frac{1}{2!} \left(\int_b \hat{q}(\vec{b}) G_1(\vec{b}; \tau) + \frac{1}{2!} \int_{b_1, b_2} \hat{q}(\vec{b}_1) \hat{q}(\vec{b}_2) G_2(\vec{b}_1, \vec{b}_2; \tau) + \dots\right)^2 + \\
&\quad \left. - \frac{1}{3!} \left(\int_b \hat{q}(\vec{b}) G_1(\vec{b}; \tau) + \frac{1}{2!} \int_{b_1, b_2} \hat{q}(\vec{b}_1) \hat{q}(\vec{b}_2) G_2(\vec{b}_1, \vec{b}_2; \tau) + \dots\right)^3 + \dots\right\} |\psi(0)\rangle.
\end{aligned} \tag{86}$$

The lowering and raising operators in principle depend on b and τ , but in what follows we disregard the τ dependence. The idea is to replace Eq.(82) in Eq.(81) and regroup all the terms with the same order in \hat{q} . The left-hand side of Schrödinger equation leads to

$$\begin{aligned}
\frac{\partial}{\partial \tau} |\psi(\tau)\rangle &= \left\{ - \int_b \hat{q}(\vec{b}) \frac{\partial}{\partial \tau} G_1(\vec{b}; \tau) \right. \\
&\quad - \frac{1}{2!} \int_{b_1, b_2} \hat{q}(\vec{b}_1) \hat{q}(\vec{b}_2) \left[\frac{\partial}{\partial \tau} G_2(\vec{b}_1, \vec{b}_2; \tau) - \frac{\partial}{\partial \tau} (G_1(\vec{b}_1; \tau) G_1(\vec{b}_2; \tau)) \right] + \\
&\quad - \frac{1}{3!} \int_{b_1, b_2, b_3} \hat{q}(\vec{b}_1) \hat{q}(\vec{b}_2) \hat{q}(\vec{b}_3) \left[\frac{\partial}{\partial \tau} G_3(\vec{b}_1, \vec{b}_2, \vec{b}_3; \tau) - \frac{3}{2!} \frac{\partial}{\partial \tau} (G_1(\vec{b}_1; \tau) G_2(\vec{b}_2, \vec{b}_3; \tau)) \right. \\
&\quad \left. \left. - \frac{3}{2!} \frac{\partial}{\partial \tau} (G_1(\vec{b}_3; \tau) G_2(\vec{b}_1, \vec{b}_2; \tau)) + \frac{\partial}{\partial \tau} (G_1(\vec{b}_1; \tau) G_1(\vec{b}_2; \tau) G_1(\vec{b}_3; \tau)) \right] + \dots \right\}.
\end{aligned} \tag{87}$$

The first term in the Hamiltonian on the right-hand side of Eq.(81) gives

$$\begin{aligned}
& -\epsilon_{\mathcal{P}} \left\{ \int_b \hat{q}(b) G_1(\vec{b}; \tau) + \int_{b_1, b_2} \hat{q}(b_1) \hat{q}(b_2) \left[G_2(\vec{b}_2, \vec{b}_1; \tau) - G_1(\vec{b}_1; \tau) G_1(\vec{b}_2; \tau) \right] + \right. \\
& \quad \left. + \frac{1}{3!} \int_{b_1, b_2, b_3} \hat{q}(b_1) \hat{q}(b_2) \hat{q}(b_3) [\dots] + \dots \right\}
\end{aligned} \tag{88}$$

The interaction part leads to

$$\begin{aligned}
& \lambda \left\{ - \int_b \hat{q}(b) \left[G_2(\vec{b}, \vec{b}; \tau) - G_1(\vec{b}; \tau) G_1(\vec{b}; \tau) \right] \right. \\
& \quad + \int_{b_1, b_2} \hat{q}(b_1) \hat{q}(b_2) \left[G_1(\vec{b}_1) \delta(\vec{b}_1 - \vec{b}_2) + G_3(\vec{b}_2, \vec{b}_1, \vec{b}_1) - 2G_1(\vec{b}_1) G_2(\vec{b}_1, \vec{b}_2) + \right. \\
& \quad \left. - G_1(\vec{b}_2) G_2(\vec{b}_1, \vec{b}_1) + G_1(\vec{b}_2) G_1(\vec{b}_1) G_1(\vec{b}_1) \right] + \frac{1}{3!} \int_{b_1, b_2, b_3} \hat{q}(b_1) \hat{q}(b_2) \hat{q}(b_3) [\dots] + \dots \left. \right\}
\end{aligned} \tag{89}$$

Regrouping order-by-order leads to an infinity set of coupled differential equations. To derive the above equations the commutator (80) was used. The first two coupled differential equations are

$$\frac{\partial}{\partial \tau} G_1(\vec{b}; \tau) = \epsilon_{\mathcal{P}} \left[1 + \frac{\lambda}{\epsilon_{\mathcal{P}}} G_1(\vec{b}; \tau) \right] G_1(\vec{b}; \tau) - \lambda G_2(\vec{b}, \vec{b}; \tau) \tag{90}$$

and

$$\begin{aligned} \frac{\partial}{\partial \tau} G_2(\vec{b}_1, \vec{b}_2; \tau) &= 2\epsilon_{\mathcal{P}} G_2(\vec{b}_1, \vec{b}_2; \tau) + 4\lambda G_1(\vec{b}_1; \tau) G_2(\vec{b}_1, \vec{b}_2; \tau) \\ &\quad - 2\lambda G_1(\vec{b}_1; \tau) \delta(\vec{b}_1 - \vec{b}_2) - 2\lambda G_3(\vec{b}_1, \vec{b}_1, \vec{b}_2) \end{aligned} \quad (91)$$

The structure of the evolution equations derived from RFT naturally leads to a hierarchy of coupled differential equations for correlation functions. For example, the equation for $G_1(\vec{b}, \tau)$ function is coupled to $G_2(\vec{b}, \vec{b}', \tau)$ function via a non-linear interaction term, while $G_2(\vec{b}, \vec{b}', \tau)$ function is itself coupled to both $G_1(\vec{b}, \tau)$ and higher-order, $G_3(\vec{b}, \vec{b}', \vec{b}'', \tau)$, correlation functions. This cascade of couplings originates from expanding the theory in powers of the reggeon fields q , where non-linear interaction terms generate correlations at increasing orders.

A closely related phenomenon occurs in high-energy QCD, particularly in the small- x regime, where the JIMWLK equation [14, 19–26] governs the evolution of Wilson line operators, gauge-invariant correlators that encode the scattering of partons off a dense target. Like in RFT, the JIMWLK equation defines a functional evolution in rapidity for a probability distribution of Wilson lines, and when projected onto correlators (e.g., dipole or quadrupole operators), it gives rise to a Balitsky hierarchy of coupled evolution equations. Each equation for an n -point function involves the $(n+1)$ -point function, reflecting the non-linear and collective nature of QCD dynamics at high energies.

The formal similarity lies in the structure of these infinite hierarchies being evolved in rapidity with the correlators depending on the transverse variables, where truncation or modeling of higher-order correlators is often needed to make the system tractable. In both cases, the hierarchy reflects the fundamental role of interactions in generating and propagating correlations, whether between reggeon fields in RFT or Wilson lines in JIMWLK/QCD. This analogy offers a conceptual bridge between non-perturbative approaches to high-energy scattering in QCD and more general field-theoretic descriptions of Reggeon dynamics.

For our purpose we can neglect the higher-order correlation functions, which corresponds to taking the semi-classical approximation, transforming the operator (83) into the classical action as was done in appendix A of Ref. [50]. This procedure leads to the equation

$$\frac{\partial}{\partial \tau} G_1(\vec{b}; \tau) = \epsilon_{\mathcal{P}} \left[1 + \frac{\lambda}{\epsilon_{\mathcal{P}}} G_1(\vec{b}; \tau) \right] G_1(\vec{b}; \tau) . \quad (92)$$

Our approach consists in identifying the proportionality between the 2-point correlation function and the scattering amplitude in b -space.

$$G_1(\vec{b}, \tau) \sim i \tilde{T}(b, \tau) . \quad (93)$$

Noting here that G_1 is complex, this leads to Eq.(15).

B Calculation and some useful integrals

B.1 Integrals for total cross section for pure imaginary amplitudes

To calculate the forward imaginary amplitude from a purely Gaussian imaginary profile we have

$$K_1 = \int b db \frac{B e^{-\beta b^2}}{C + D e^{-\beta b^2}} \quad (94)$$

Changing $u = e^{-\beta b^2} \implies du = -2\beta b e^{-\beta b^2} db$ we obtain

$$K_1 = -\frac{B}{2\beta} \int \frac{du}{C + D u} = -\frac{B}{2D\beta} \log(C + D e^{-\beta b^2}) . \quad (95)$$

The forward imaginary amplitude for a purely exponential profile is given by the integral

$$K_2 = \int b db \frac{B e^{-\beta b}}{C + D e^{-\beta b}} \quad (96)$$

Changing $u = e^{-\beta b} \implies du = -\beta b e^{-\beta b} db$ and $b = -\frac{\log u}{\beta}$. Our integral becomes

$$K_2 = \frac{1}{\beta^2} \int du \frac{\log u}{C + D u} . \quad (97)$$

Integrating by parts we change $u' = \log u \implies du' = \frac{du}{u}$ and $dv' = \frac{du}{C + D u} \implies v' = \log(C + D u)$ and we obtain

$$\begin{aligned} K_2 &= \frac{1}{\beta^2} \left(\log u \log(C + D u) - \int du \frac{\log(C + D u)}{u} \right) \\ &= \frac{1}{\beta^2} \left[\log u \log(C + D u) - \left(\text{Li}_2\left(\frac{D u}{C} + 1\right) + \log\left(-\frac{D u}{C}\right) \log(C + D u) \right) \right] \\ &= -\frac{1}{\beta^2} \left(\text{Li}_2\left(\frac{D e^{-\beta b}}{C} + 1\right) + \log\left(-\frac{D}{C}\right) \log(C + D e^{-\beta b}) \right) . \end{aligned} \quad (98)$$

B.2 Integrals of the real and imaginary parts of the amplitudes at $t = 0$ for Gaussian profiles

To calculate the forward real and imaginary amplitudes in t space we need the integrals

$$I_1 = \int b db \frac{A e^{-\beta b^2}}{(B e^{-\beta b^2} + D)^2 + C} \quad (99)$$

Changing $u = e^{-\beta b^2} \implies du = -2\beta b e^{-\beta b^2} db$ and the integral becomes

$$I_1 = -\frac{A}{2\beta} \int \frac{du}{(Bu + D)^2 + C} = -\frac{A}{2B\sqrt{C}b} \tan^{-1} \left(\frac{B e^{-\beta b^2} + D}{\sqrt{C}} \right) \quad (100)$$

The second kind of integral is

$$I_2 = \int b db \frac{A}{(B e^{-\beta b^2} + D)^2 + C} \quad (101)$$

As before, we change $u = e^{-\beta b^2} \implies du = -2\beta b e^{-\beta b^2} db$ and the integral becomes

$$I_2 = -\frac{A}{2\beta} \int \frac{du}{u((Bu + D)^2 + C)} \quad (102)$$

Changing $v = Bu + D \implies dv = B du$ and the integral becomes

$$\begin{aligned} I_2 &= -\frac{A}{2\beta} \int \frac{dv}{(v - D)(v^2 + C)} = -\frac{A}{2\beta} \int \frac{dv}{(C + D^2)} \left(\frac{-D - v}{v^2 + C} + \frac{1}{v - D} \right) \\ &= \frac{A}{2\beta((B e^{-\beta b^2} + D)^2 + C)} \left(\frac{D}{\sqrt{C}} \tan^{-1} \left(\frac{B e^{-\beta b^2} + D}{\sqrt{C}} \right) - \log \frac{(B e^{-\beta b^2})}{(C + (B e^{-\beta b^2} + D)^2)^{\frac{1}{2}}} \right) \end{aligned} \quad (103)$$

where we make a fraction decomposition leading to easy integrals to be solved.

Separating the real and imaginary parts of Eq. (16), and applying Eq. (46) as initial condition, we calculate

$$\begin{aligned} T_R(\tau, t = 0) &= \int_0^\infty b db \tilde{T}_{0R}(\tau, b) \\ &= \int_0^\infty b db \frac{\tilde{T}_{0R}(b) \left[\left(1 - \frac{\lambda}{\epsilon_P} \tilde{T}_{0I}(b) \right) e^{-\epsilon_P \Delta\tau} + \frac{\lambda}{\epsilon_P} \tilde{T}_{0I}(b) \right] + \frac{\lambda}{\epsilon_P} \tilde{T}_{0R}(b) \tilde{T}_{0I}(b) (e^{-\epsilon_P \Delta\tau} - 1)}{\left[\left(1 - \frac{\lambda}{\epsilon_P} \tilde{T}_{0I}(b) \right) e^{-\epsilon_P \Delta\tau} + \frac{\lambda}{\epsilon_P} \tilde{T}_{0I}(b) \right]^2 + \frac{\lambda^2}{\epsilon_P^2} \tilde{T}_{0R}(b)^2 (1 - e^{-\epsilon_P \Delta\tau})^2} \\ &= \int_0^\infty b db \frac{A \left[\left(e^{\beta b^2} - \frac{\lambda}{\epsilon_P} B \right) e^{-\epsilon_P \Delta\tau} + \frac{\lambda}{\epsilon_P} B \right] - \frac{\lambda}{\epsilon_P} AB (1 - e^{-\epsilon_P \Delta\tau})}{\left[\left(e^{\beta b^2} - \frac{\lambda}{\epsilon_P} B \right) e^{-\epsilon_P \Delta\tau} + \frac{\lambda}{\epsilon_P} B \right]^2 + \frac{\lambda^2}{\epsilon_P^2} A^2 (1 - e^{-\epsilon_P \Delta\tau})^2} \\ &= \frac{\epsilon_P e^{\epsilon_P \Delta\tau}}{4\beta\lambda(e^{\epsilon_P \Delta\tau} - 1)} \left(\pi + 2 \tan^{-1} \left(\frac{\epsilon_P - B\lambda + B\lambda e^{\epsilon_P \Delta\tau}}{A\lambda(1 - e^{\epsilon_P \Delta\tau})} \right) \right), \end{aligned} \quad (104)$$

$$\begin{aligned}
T_I(\tau, t=0) &= \int_0^\infty b db \tilde{T}_{0I}(\tau, b) \\
&= \int_0^\infty b db \frac{\tilde{T}_{0I}(b) \left[\left(1 - \frac{\lambda}{\epsilon_P} \tilde{T}_{0I}(b)\right) e^{-\epsilon_P \Delta\tau} + \frac{\lambda}{\epsilon_P} \tilde{T}_{0I}(b) \right] - \frac{\lambda}{\epsilon_P} \tilde{T}_{0R}(b)^2 (e^{-\epsilon_P \Delta\tau} - 1)}{\left[\left(1 - \frac{\lambda}{\epsilon_P} \tilde{T}_{0I}(b)\right) e^{-\epsilon_P \Delta\tau} + \frac{\lambda}{\epsilon_P} \tilde{T}_{0I}(b) \right]^2 + \frac{\lambda^2}{\epsilon_P^2} \tilde{T}_{0R}(b)^2 (1 - e^{-\epsilon_P \Delta\tau})^2} \\
&= \int_0^\infty b db \frac{B \left[\left(e^{\beta b^2} - \frac{\lambda}{\epsilon_P} B\right) e^{-\epsilon_P \Delta\tau} + \frac{\lambda}{\epsilon_P} B \right] + \frac{\lambda}{\epsilon_P} A^2 (1 - e^{-\epsilon_P \Delta\tau})}{\left[\left(e^{\beta b^2} - \frac{\lambda}{\epsilon_P} B\right) e^{-\epsilon_P \Delta\tau} + \frac{\lambda}{\epsilon_P} B \right]^2 + \frac{\lambda^2}{\epsilon_P^2} A^2 (1 - e^{-\epsilon_P \Delta\tau})^2} \\
&= \frac{\epsilon_P e^{\epsilon_P \Delta\tau}}{4\beta\lambda(e^{\epsilon_P \Delta\tau} - 1)} \log \left(1 + \frac{2B\lambda}{\epsilon_P} (e^{\epsilon_P \Delta\tau} - 1) + (A^2 + B^2) \frac{\lambda^2}{\epsilon_P^2} (e^{\epsilon_P \Delta\tau} - 1)^2 \right) \quad (105)
\end{aligned}$$

C Acknowledgments

This paper is dedicated to my daughter, Josephine, whose curiosity and joy are a constant source of inspiration. I especially thank Erasmo Ferreira, Pedro C. Malta, Piotr Kotko and Cyrille Marquet for reading the manuscript, engaging in discussions, and offering important suggestions. I also thank Dr. Said Mazen for interesting discussions regarding the mathematical aspects of the differential equations. I gratefully acknowledge the AGH University of Science and Technology for its hospitality during the early stages of this project. Finally, I acknowledge the support of the National Science Centre in Poland, grant no. 2020/37/K/ST2/02665 and the Norwegian Financial Mechanism, during the period from 2021 to 2023, when the initial ideas for this project were developed.

References

- [1] S. Donnachie, G. Dosch, P. Landshoff, and O. Nachtmann. *Pomeron Physics and QCD*. Cambridge Monographs on Particle Physics, Nuclear Physics and Cosmology. Cambridge University Press, 2002.
- [2] G. F. Chew and S. C. Frautschi. Regge trajectories and the principle of maximum strength for strong interactions. *Phys. Rev. Lett.*, 8:41–44, 1962.
- [3] T. Kinoshita. Pomeranchuk-like theorem that can be proved. *Phys. Rev. D*, 2:2346–2348, 1970.
- [4] M. Froissart. Asymptotic behavior and subtractions in the Mandelstam representation. *Phys. Rev.*, 123:1053–1057, 1961.
- [5] A. Martin. Extension of the axiomatic analyticity domain of scattering amplitudes by unitarity-I. *Nuovo Cimento*, 42:930–953, 1966.
- [6] H. Cheng and T. T. Wu. Limit of Cross-Sections at Infinite Energy. *Phys. Rev. Lett.*, 24:1456–1460, 1970.

- [7] A. S. Carroll et al. Total Cross-Sections of p and \bar{p} on Protons and Deuterons Between 50-GeV/c and 200-GeV/c. *Phys. Rev. Lett.*, 33:928, 1974.
- [8] D. Amati, L. Caneschi, and R. Jengo. Summing pomeron trees. *Nucl. Phys. B*, 101(2):397–410, 1975.
- [9] H. Kakkad, A. K. Kohara, and P. Kotko. Evolution equation for elastic scattering of hadrons. *Eur. Phys. J. C*, 82(9):830, 2022.
- [10] R. A. Fisher. The wave of advance of advantageous genes. *Ann. Eugen.*, 7(4):355–369, 1937.
- [11] A. Kolmogorov, I. Petrovsky, and N. Piscounov. *Moscou Univ. Bull. Math. A*, 1(1):1, 1937.
- [12] M. J. Ablowitz and A. Zeppetella. Explicit solutions of Fisher’s equation for a special wave speed. *Bull. Math. Biol.*, 41(9):835, 1979.
- [13] S. Munier and R. B. Peschanski. Geometric scaling as traveling waves. *Phys. Rev. Lett.*, 91:232001, 2003.
- [14] I. Balitsky. Operator expansion for high-energy scattering. *Nucl. Phys. B*, 463:99–160, 1996.
- [15] Yuri V. Kovchegov. Small x F_2 structure function of a nucleus including multiple pomeron exchanges. *Phys. Rev. D*, 60:034008, 1999.
- [16] C. Marquet, R. B. Peschanski, and G. Soyez. Traveling waves and geometric scaling at non-zero momentum transfer. *Nucl. Phys. A*, 756:399–418, 2005.
- [17] Y. V. Kovchegov, L. Szymanowski, and S. Wallon. Perturbative odderon in the dipole model. *Phys. Lett. B*, 586:267–281, 2004.
- [18] V. Gribov. *Strong Interactions of Hadrons at High Energies: Gribov Lectures on Theoretical Physics*. Cambridge University Press, 2008.
- [19] J. Jalilian-Marian et al. The BFKL equation from the Wilson renormalization group. *Nucl. Phys. B*, 504:415–431, 1997.
- [20] J. Jalilian-Marian et al. The Wilson renormalization group for low x physics: Towards the high density regime. *Phys. Rev. D*, 59:014014, 1998.
- [21] J. Jalilian-Marian, A. Kovner, and H. Weigert. The Wilson renormalization group for low x physics: Gluon evolution at finite parton density. *Phys. Rev. D*, 59:014015, 1998.
- [22] A. Kovner, J. G. Milhano, and H. Weigert. Relating different approaches to nonlinear QCD evolution at finite gluon density. *Phys. Rev. D*, 62:114005, 2000.

- [23] A. Kovner and J. G. Milhano. Vector potential versus color charge density in low x evolution. *Phys. Rev. D*, 61:014012, 2000.
- [24] H. Weigert. Unitarity at small Bjorken x . *Nucl. Phys. A*, 703:823–860, 2002.
- [25] E. Iancu, A. Leonidov, and L. McLerran. Nonlinear gluon evolution in the color glass condensate. 1. *Nucl. Phys. A*, 692:583–645, 2001.
- [26] E. Ferreiro, E. Iancu, A. Leonidov, and L. McLerran. Nonlinear gluon evolution in the color glass condensate. 2. *Nucl. Phys. A*, 703:489–538, 2002.
- [27] J. R. Forshaw and D. A. Ross. *Quantum Chromodynamics and the Pomeron*. Cambridge University Press, 2011.
- [28] A. Kovner and M. Lublinsky. Odderon and seven Pomerons: QCD Reggeon field theory from JIMWLK evolution. *JHEP*, 02:058, 2007.
- [29] T. Altinoluk, A. Kovner, M. Lublinsky, and J. Peressutti. QCD Reggeon Field Theory for every day: Pomeron loops included. *JHEP*, 03:109, 2009.
- [30] A. Donnachie and P. V. Landshoff. Total cross-sections. *Phys. Lett. B*, 296:227–232, 1992.
- [31] A. K. Kohara, E. Ferreira, T. Kodama, and M. Rangel. Elastic amplitudes studied with the LHC measurements at 7 and 8 TeV. *Eur. Phys. J. C*, 77(12):877, 2017.
- [32] A. K. Kohara, E. Ferreira, and M. Rangel. The interplay of hadronic amplitudes and Coulomb phase in LHC measurements at 13 TeV. *Phys. Lett. B*, 789:1–6, 2019.
- [33] A. K. Kohara, E. Ferreira, and T. Kodama. pp Elastic Scattering at LHC Energies. *Eur. Phys. J. C*, 74:3175, 2014.
- [34] H. G. Dosch, E. Ferreira, and A. Kramer. Nonperturbative QCD treatment of high-energy hadron-hadron scattering. *Phys. Rev. D*, 50:1992–2015, 1994.
- [35] C. Bourrely, J. Soffer, and Tai Tsun Wu. New impact picture for low- and high-energy proton-proton elastic scattering. *Phys. Rev. D*, 19:3249–3260, 1979.
- [36] A. Donnachie and P. V. Landshoff. pp and $\bar{p}p$ total cross sections and elastic scattering. *Phys. Lett. B*, 727:500–505, 2013.
- [37] A. Bialas and A. Bzdak. Wounded quarks and diquarks in heavy ion collisions. *Phys. Lett. B*, 649:263–268, 2007.
- [38] F. Nemes and T. Csorgo. Detailed Analysis of pp Elastic Scattering Data in the Quark-Diquark Model from $\sqrt{s} = 23.5$ GeV to 7 TeV. *Int. J. Mod. Phys. A*, 27:1250175, 2012.

- [39] T. Csorgo and F. Nemes. Elastic scattering of protons from $\sqrt{s} = 23.5$ GeV to 7 TeV from a generalized Bialas-Bzdak model. *Int. J. Mod. Phys. A*, 29:1450019, 2014.
- [40] A. Martin. A theorem on the real part of the high-energy scattering amplitude near the forward direction. *Phys. Lett. B*, 404:137, 1997.
- [41] A. K. Kohara. Forward scattering amplitudes of pp and $\bar{p}p$ with crossing symmetry and scaling properties. *J. Phys. G*, 46(12):125001, 2019.
- [42] R. L. Workman et al. Review of Particle Physics. *PTEP*, 2022:083C01, 2022.
- [43] E. Ferreira, A. K. Kohara, and J. Sesma. Structure of Forward pp and $\bar{p}p$ Elastic Amplitudes at Low Energies. *Phys. Rev. D*, 98(9):094029, 2018.
- [44] D. A. Fagundes, M. J. Menon, and P. V. R. G. Silva. Leading components in forward elastic hadron scattering: Derivative dispersion relations and asymptotic uniqueness. *Int. J. Mod. Phys. A*, 32(32):1750184, 2017.
- [45] R. F. Avila and M. J. Menon. Critical analysis of derivative dispersion relations at high-energies. *Nucl. Phys. A*, 744:249–272, 2004.
- [46] R. F. Avila and M. J. Menon. Derivative dispersion relations above the physical threshold. *Braz. J. Phys.*, 37:358–367, 2007.
- [47] Anderson Kendi Kohara. Observation of two zeros of the real amplitude in pp scattering at LHC energies. *Eur. Phys. J. C*, 83(2):126, 2023.
- [48] O. V. Selyugin. New properties of elastic pp and $\bar{p}p$ scattering at high energies. *Eur. Phys. J. C*, 84(6):649, 2024.
- [49] V. N. Gribov. A Reggeon diagram technique. *Zh. Eksp. Teor. Fiz.*, 53:654–672, 1967.
- [50] V. Alessandrini, D. Amati, and M. Ciafaloni. Classical Kinks and their Quantization in Supercritical Reggeon Field Theory. *Nucl. Phys. B*, 130:429–485, 1977.
- [51] H. D. I. Abarbanel et al. Reggeon field theory: formulation and use. *Phys. Rep.*, 21(3):119–182, 1975.
- [52] D. Amati et al. Reggeon field theory for $\alpha(0) > 1$. *Nucl. Phys. B*, 112(1):107–149, 1976.
- [53] V. Alessandrini, D. Amati, and R. Jengo. One-dimensional quantum theory of the pomeron. *Nucl. Phys. B*, 108(4):425–446, 1976.